Supplementary Information

A hybrid polyketide-nonribosomal peptide in nematodes that promotes larval survival

Qingyao Shou†, Likui Feng†, Yaoling Long, Jungsoo Han, Joshawna K. Nunnery, David H. Powell, Rebecca A. Butcher*

Department of Chemistry, University of Florida, Gainesville, FL 32611

†equal contributions
*Correspondence to: butcher@chem.ufl.edu

This PDF file includes:

Supplementary Figures 1-28
Supplementary Tables 1-5

Supplementary Results

Table of Contents

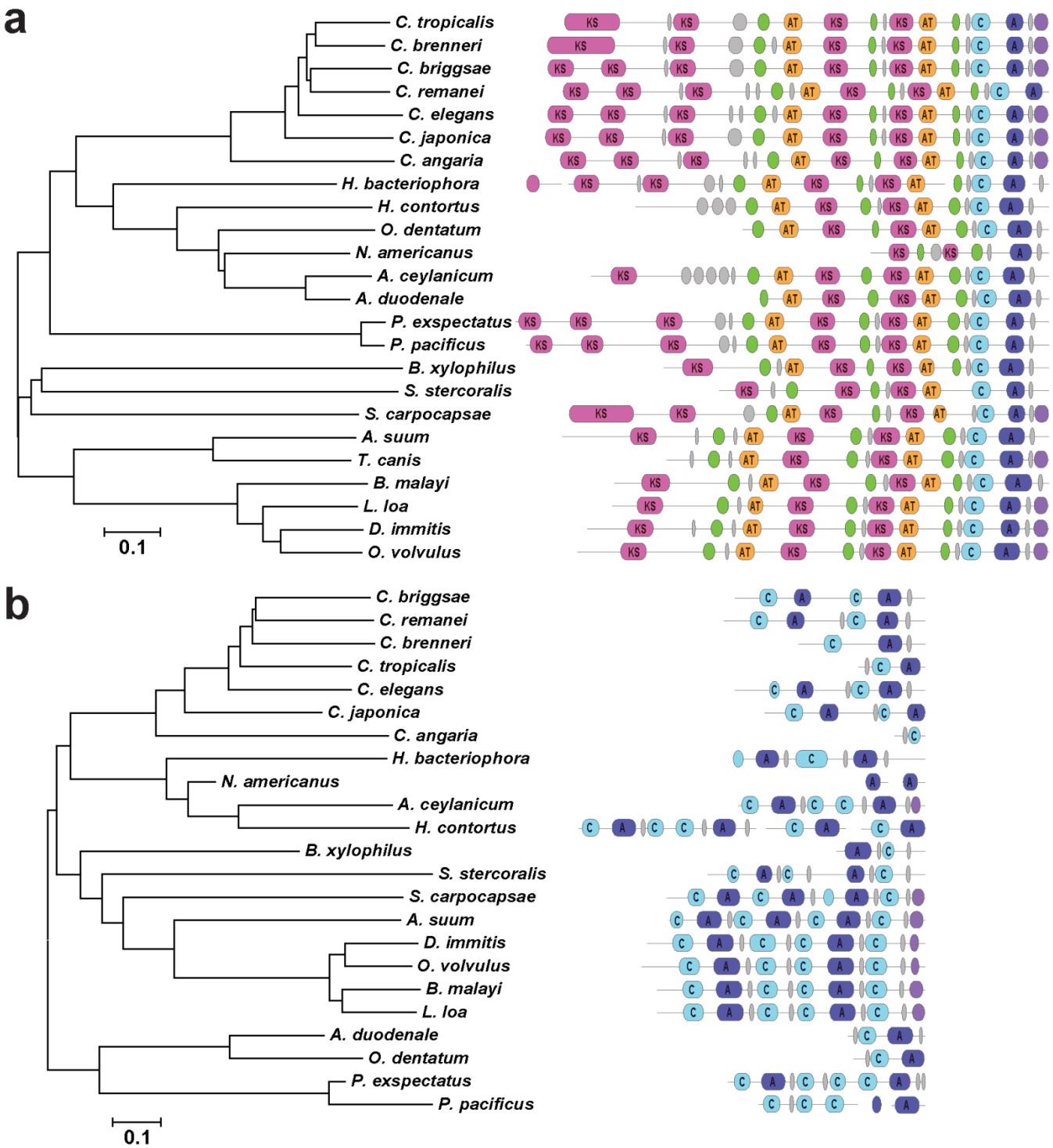

Supplementary Figure 1. Phylogeny and domain analysis of PKS-1 and NRPS-1 homologs. Phylogeny and protein domain analysis was performed as described in the methods for PKS-1 homologs (**a**) and NRPS-1 homologs (**b**) in the following nematode species: *Ancylostoma ceylanicum* (**a**, EYC37444.1; **b**, EYB85901.1), *Ancylostoma duodenale* (**a**, KIH69030.1; **b**, KIH67424.1), *Ascaris suum* (**a**, PRJNA80881; **b**, GS_05892), *Brugia malayi* (**a**, CDQ05007.1; **b**, XP_001901640.1), *Bursaphelenchus xylophilus* (**a**, BUX.s00713.159; **b**, BUX.gene.s01513.336), *Caenorhabditis angaria* (**a**, Cang_2012_03_13_00116.g4813; **b**, Cang_2012_03_13_00228.g7416), *C. brenneri* (**a**,

EGT30644.1; **b**, EGT46479.1), *C. briggsae* (**a**, EGT30644.1; **b**, CAP32083.2), *C. elegans* (**a**, NP_508923.2; **b**, CAC70135.3), *C. japonica* (**a**, CJA00126; **b**, CJA13923), *C. remanei* (**a**, XP_003118401.1; **b**, EFP02416.1), *C. tropicalis* (**a**, Csp11.Scaffold626.g6628; **b**, Csp11.Scaffold488.g2019), *Dirofilaria immitis* (**a**, nDi.2.2.2.g06619; **b**, nDi.2.2.2.g03539), *Haemonchus contortus* (**a**, CDJ83277.1; **b**, CDJ93083.1, CDJ93084.1, CDJ82649.1), *Heterorhabditis bacteriophora* (**a**, ACKM01001433.1; **b**, Hba_08702), *Loa Loa* (**a**, EJD75257.1; **b**, EFO26749.2), *Necator americanus* (**a**, ETN74557.1; **b**, NECAME_19208, NECAME_19210), *Oesophagostomum dentatum* (**a**, KHJ99846.1; **b**, KHJ98077.1), *Onchocerca volvulus* (**a**, OVOC1839; **b**, OVOC7029), *Pristionchus exspectatus* (**a**, scaffold450-EXSNAP2012.7; **b**, scaffold1344-EXSNAP2012.3), *P. pacificus* (**a**, PPA23686; **b**, PPA07616, PPA07617, PPA31783), *Steinernema carpocapsae* (**a**, L596_g18665.t1; **b**, L596_g20331.t1), *Strongyloides stercoralis* (**a**, SSTP_0001127100.1; **b**, SSTP_0000446000.1), *Toxocara canis* (**a**, KHN84567.1). If available, the Genbank accession number for the protein is listed, or, if not available, the protein name from Wormbase Parasite is listed. If a given species contained multiple proteins with homology to *pks-1* and/or *nrps-1*, the domains were annotated for all of the proteins using antiSMASH[1], but only the longest protein was used for generation of the phylogenetic tree. For the *H. bacteriophora pks-1* homolog, DNA sequence rather than protein sequence was analyzed (by first converting it to protein sequence using antiSMASH[1]). Domains depicted include ketosynthase (KS, pink), acyl carrier protein (ACP, grey), ketoreductase (KR, green), acyl transferase (AT, yellow), peptidyl carrier protein (PCP, grey), condensation (C, light blue), adenylation (A, dark purple), thioesterase (TE, light purple).

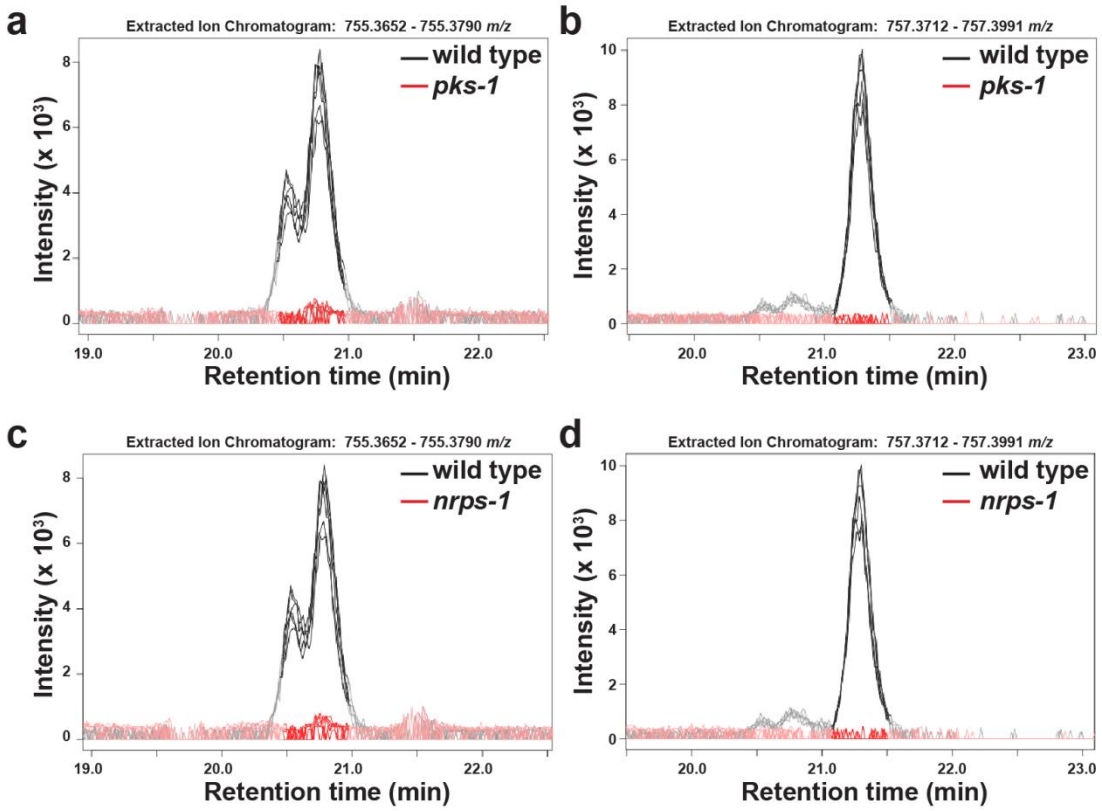

Supplementary Figure 2. Extracted ion chromatograms. Extracted ion chromatograms for *m/z* 755 (**a**,**c**) and *m/z* 757 (**b**,**d**) in wild-type versus *pks-1* mutant samples (**a**,**b**) and in wild-type versus *nrps-1* mutant samples (**c**,**d**). The *m/z* 755 feature always appears as one major and one minor peak, likely indicating two isomers. Images were generated in XCMS.[2]

Supplementary Figure 3. NMR spectra for nemamide A in dimethyl sulfoxide-d_6.
(**a**) ^{1}H NMR spectrum (with water suppression, contaminant peaks are indicated with asterisks).

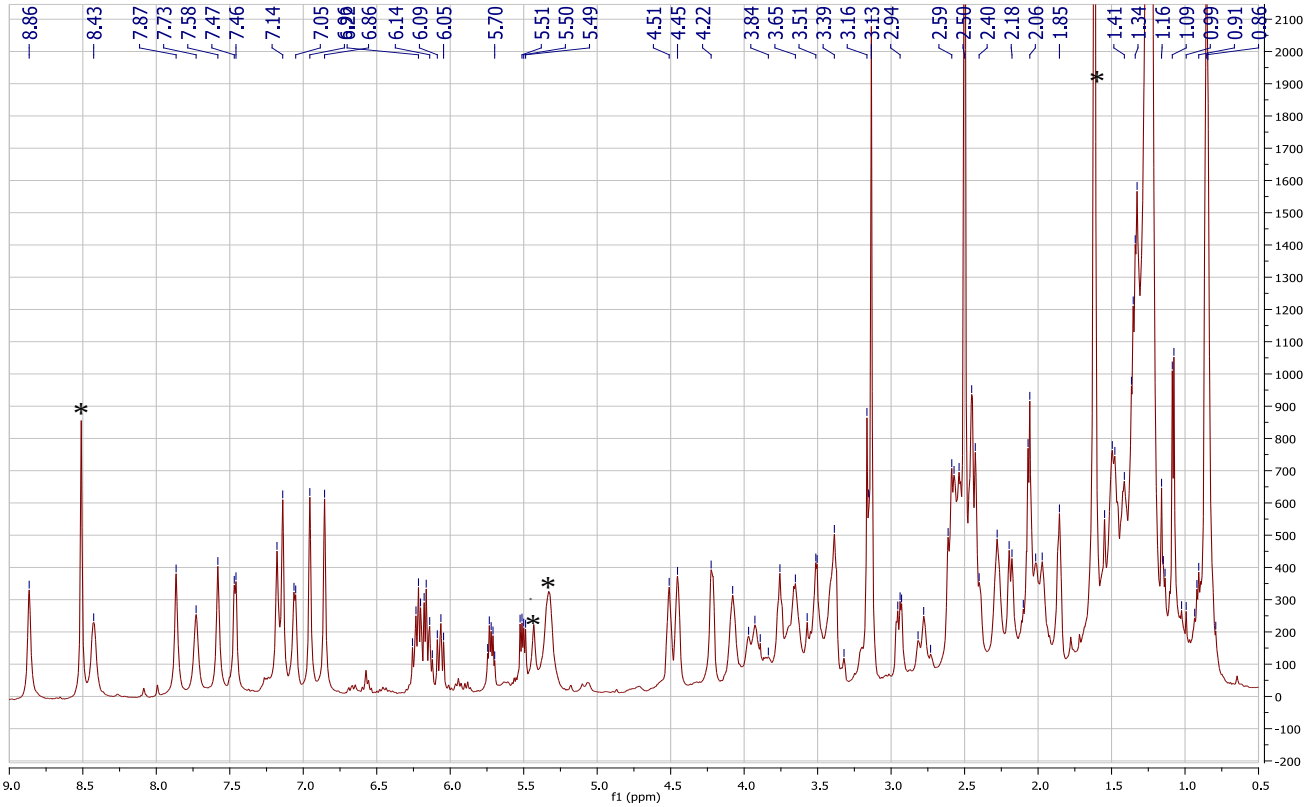

(**b**) ^{1}H NMR spectrum (without water suppression, contaminant peaks are indicated with asterisks).

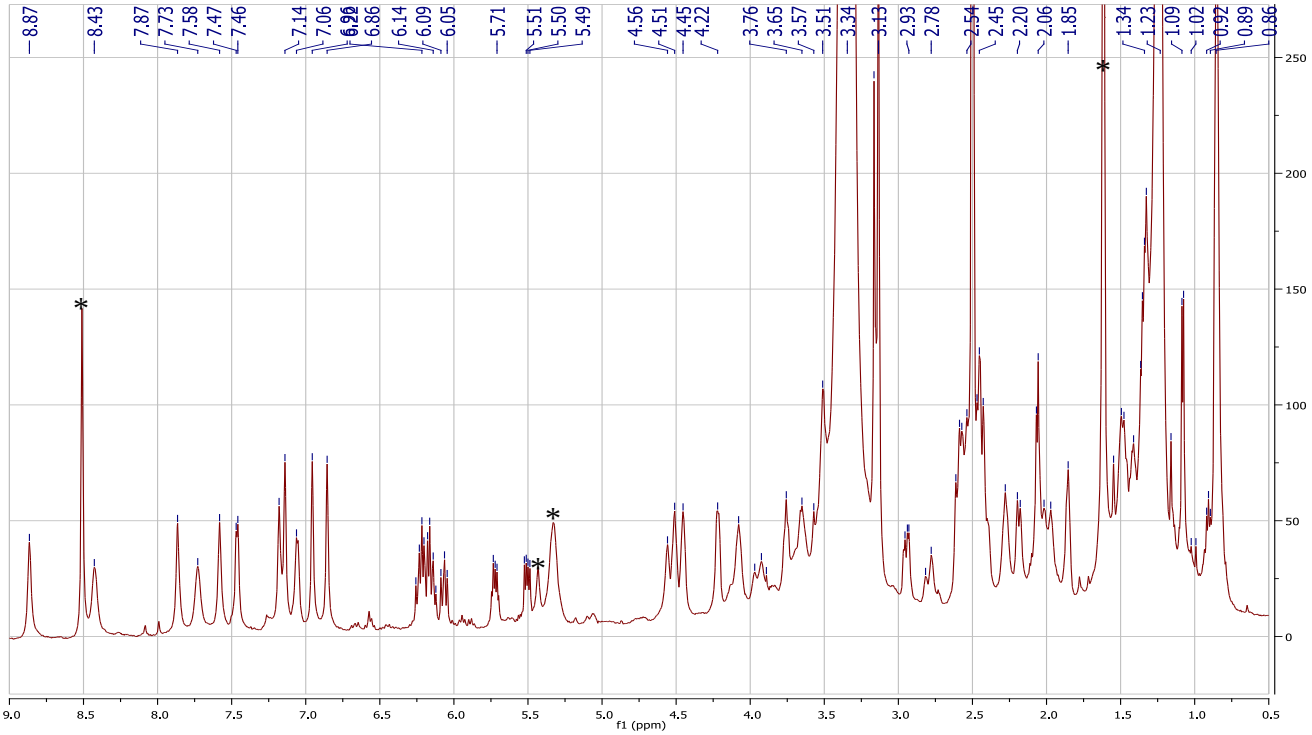

(**c**) dqf-COSY spectrum.

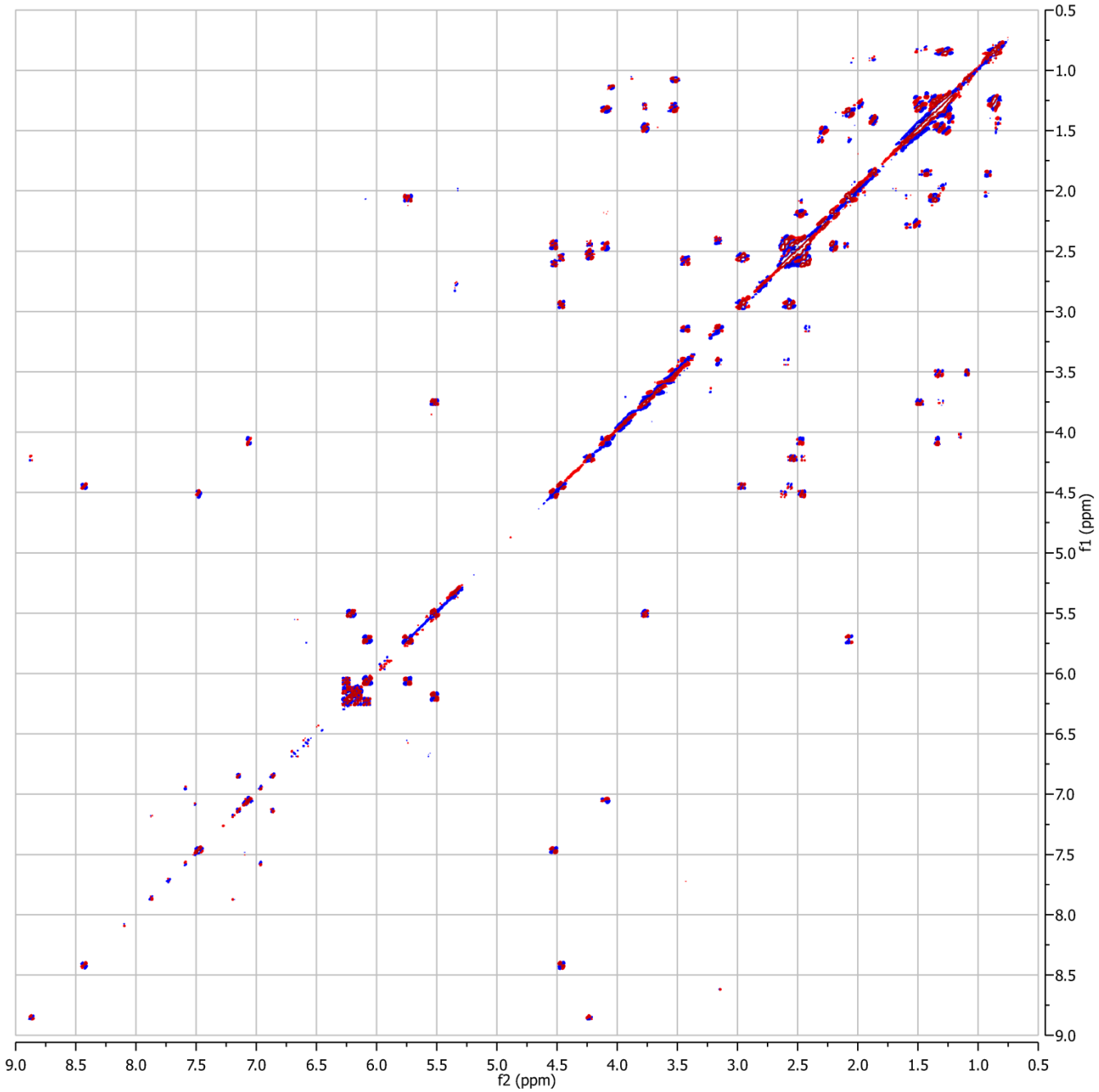

(**d**) dqf-COSY spectrum (0.5-5ppm region).

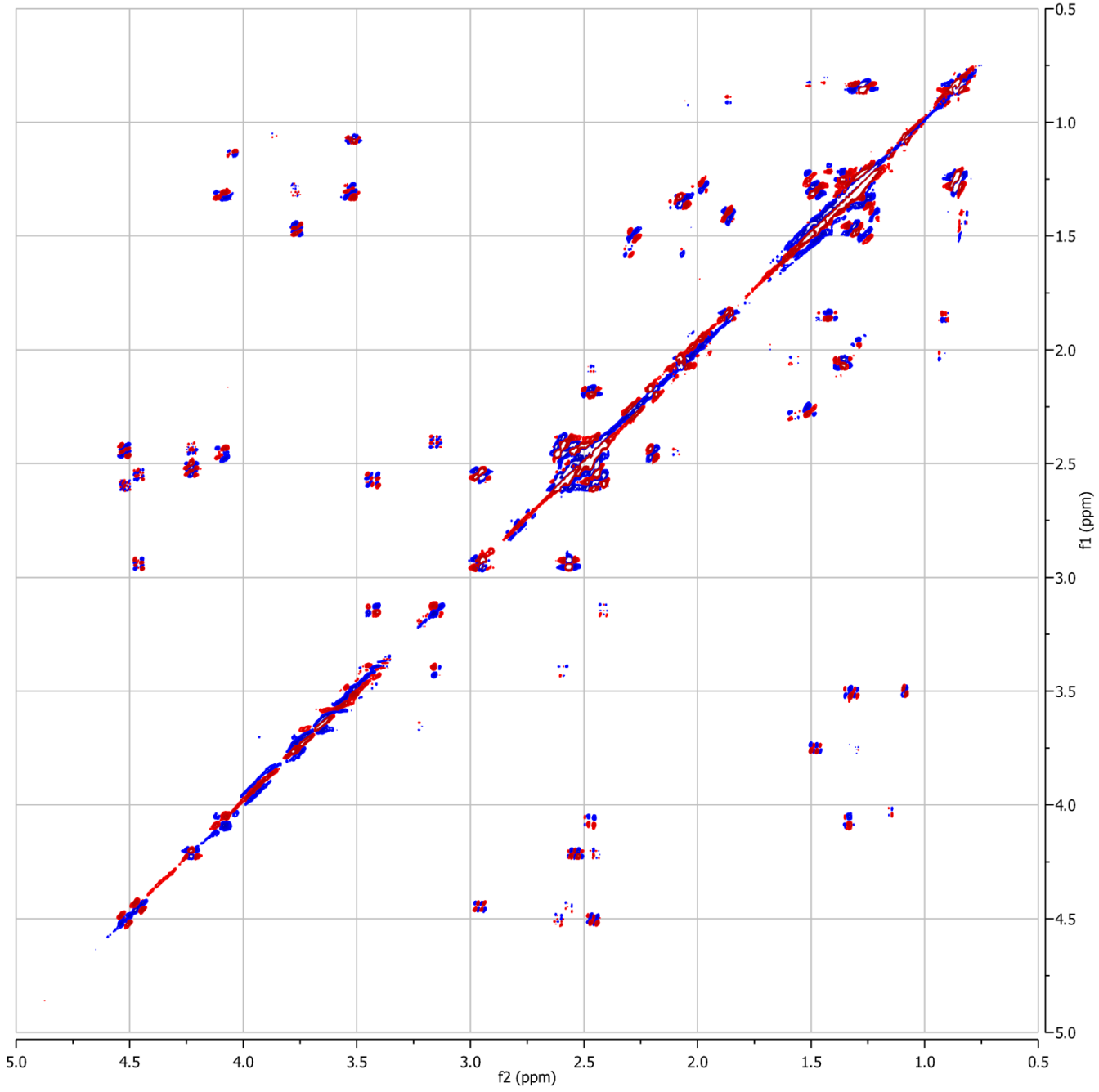

(**e**) TOCSY spectrum.

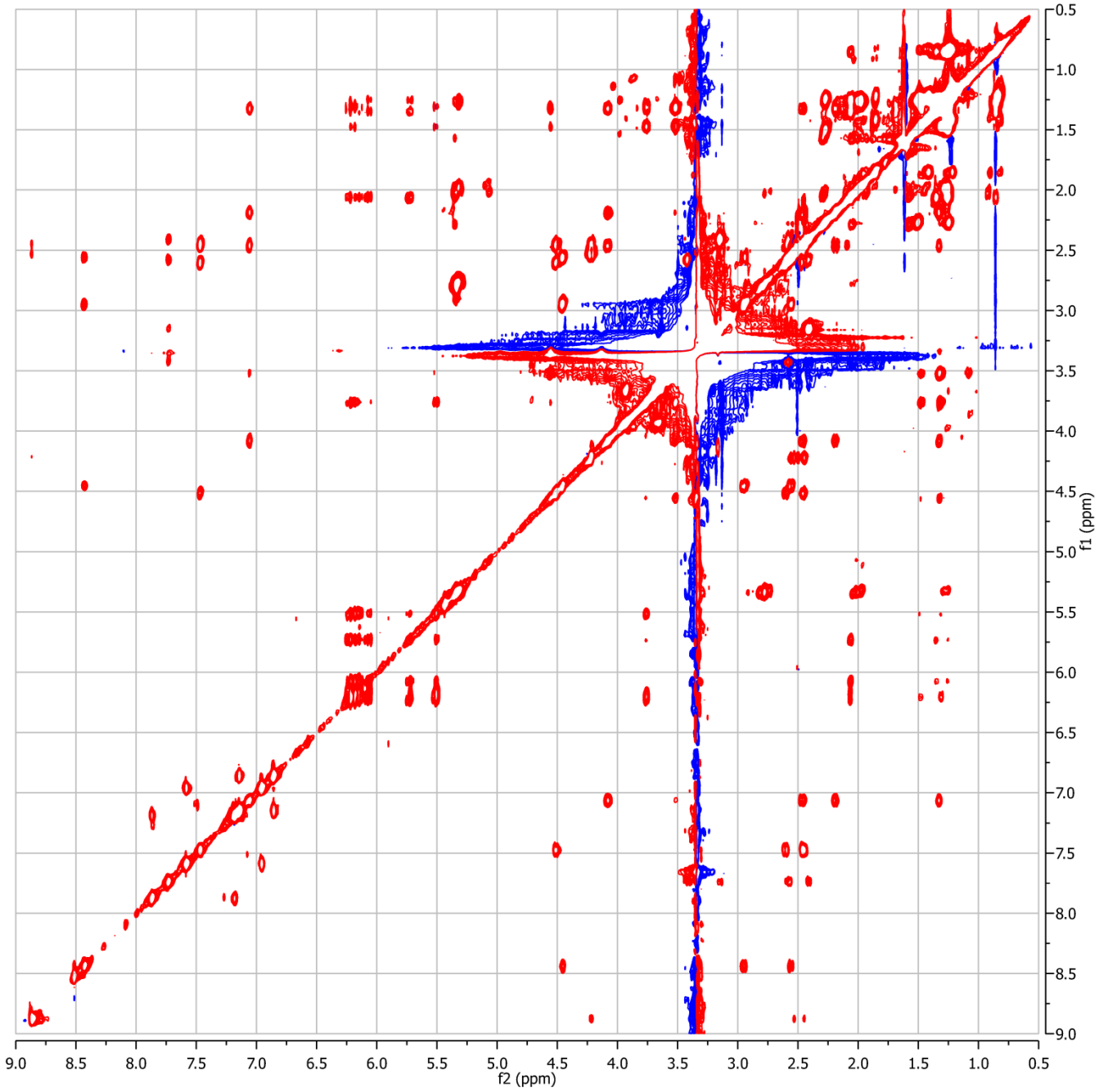

(**f**) HSQC spectrum.

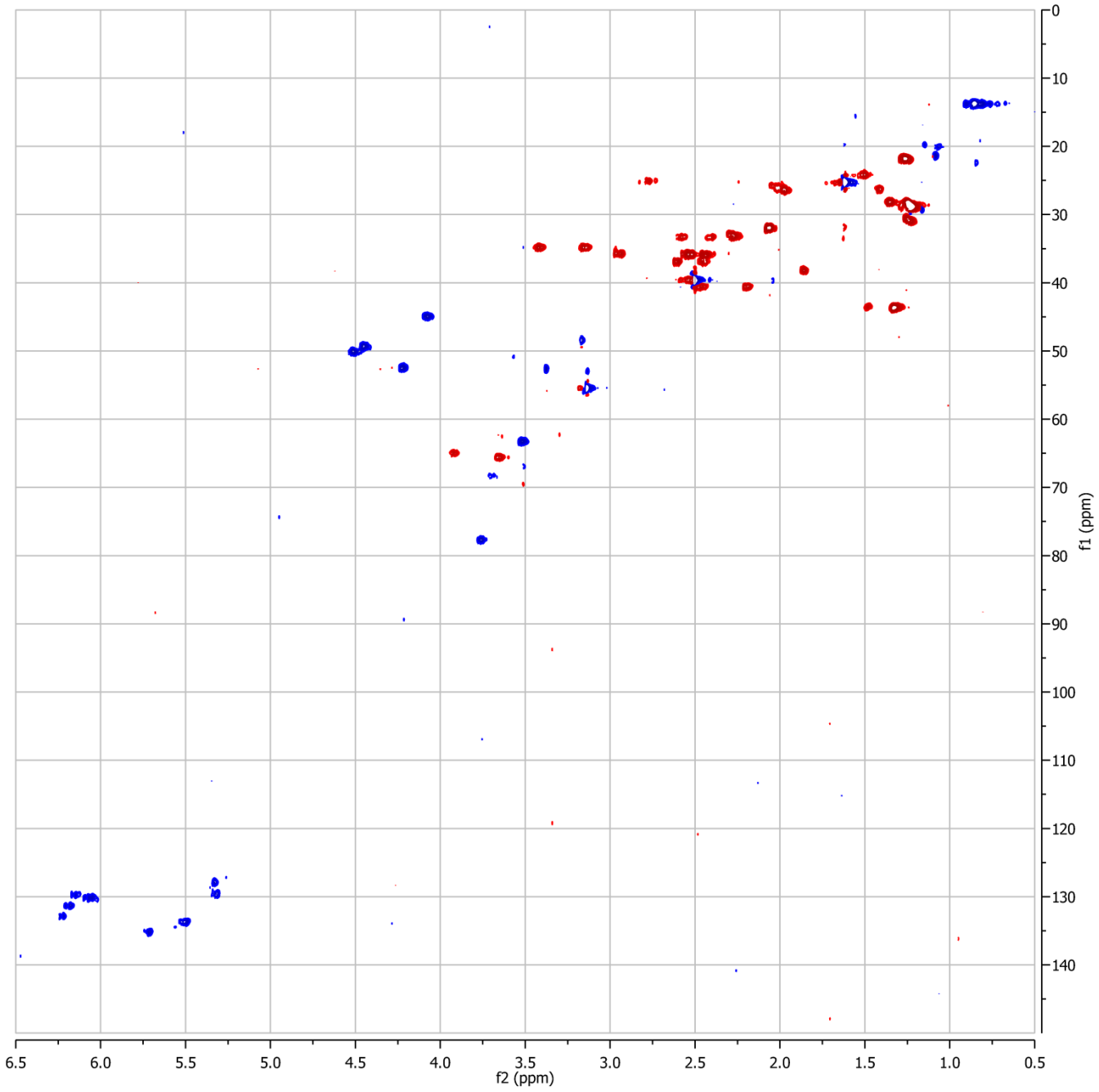

(**g**) HSQC spectrum (0.5-5ppm region).

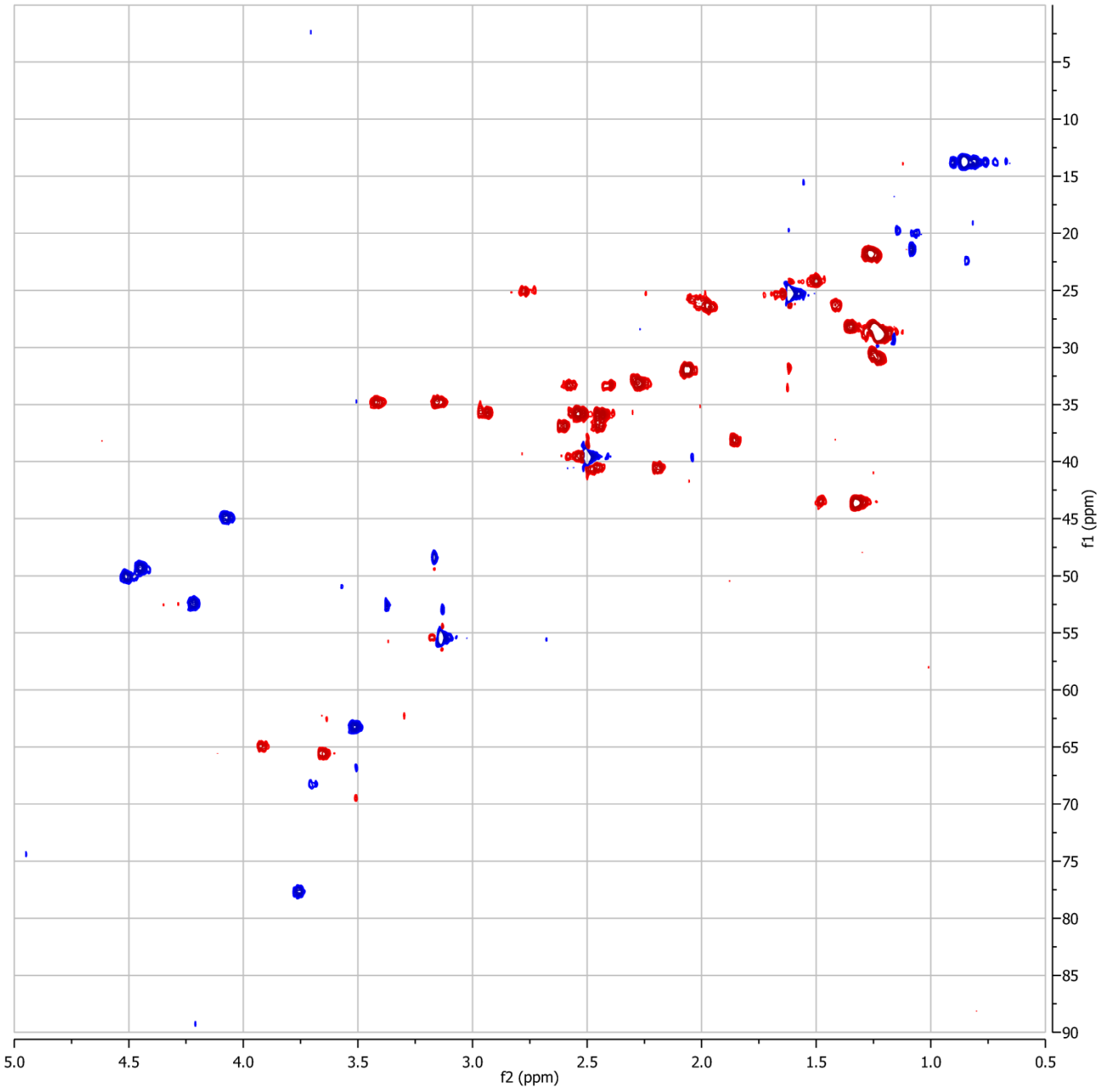

(**h**) HMBC spectrum.

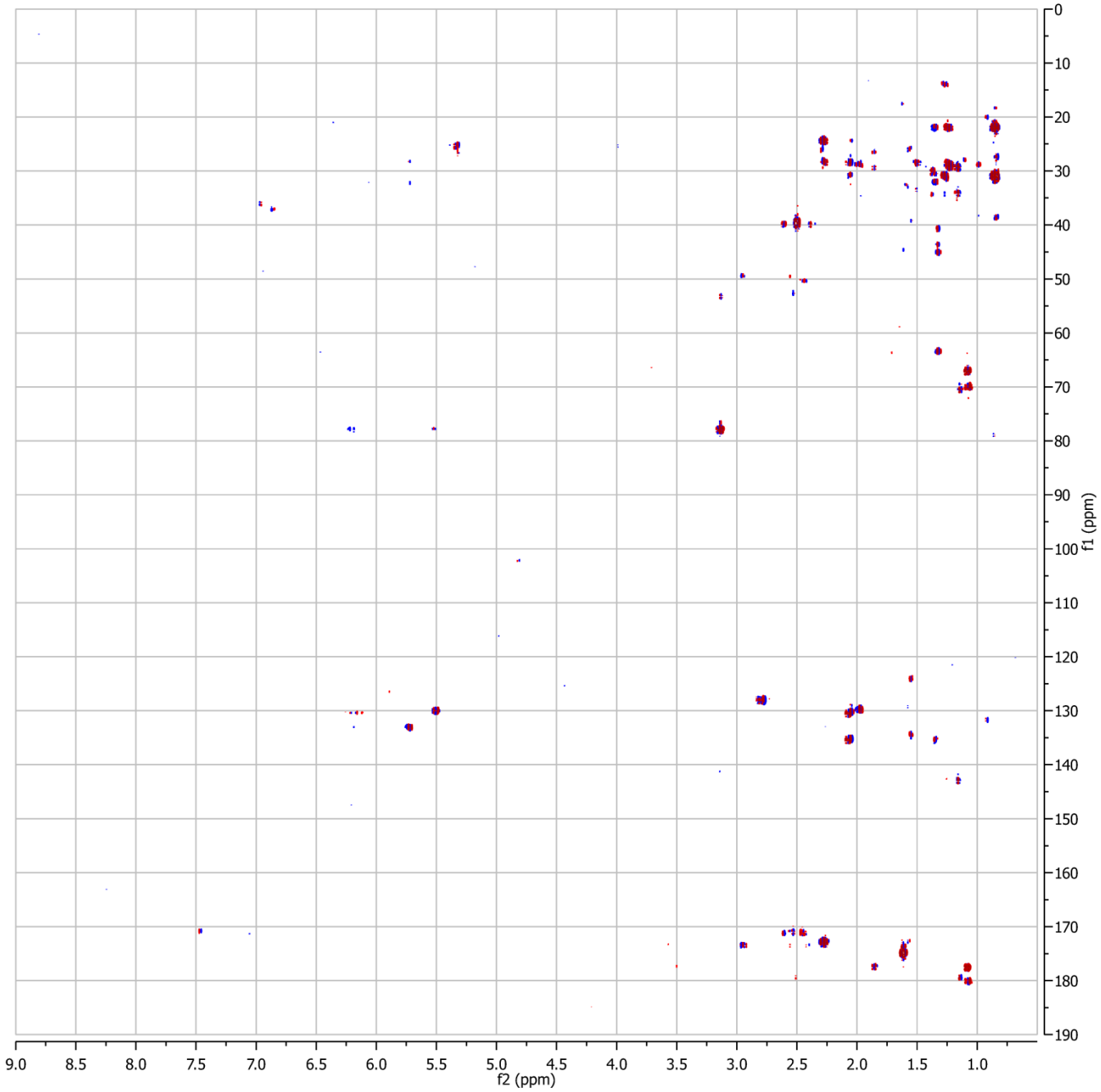

(**i**) HMBC spectrum obtained on a Bruker Avance 800 MHz NMR spectrometer.

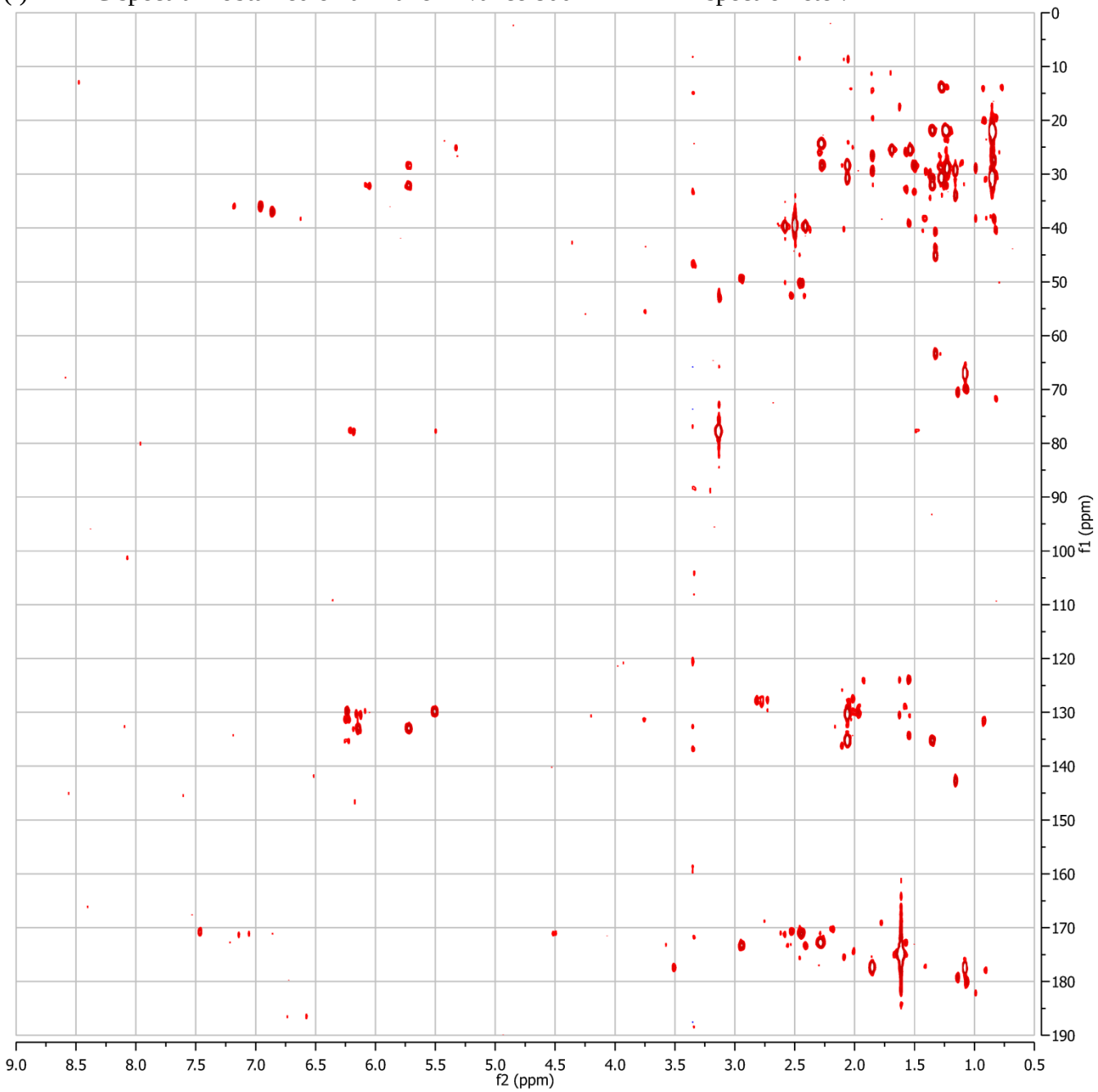

(**j**) ROESY spectrum.

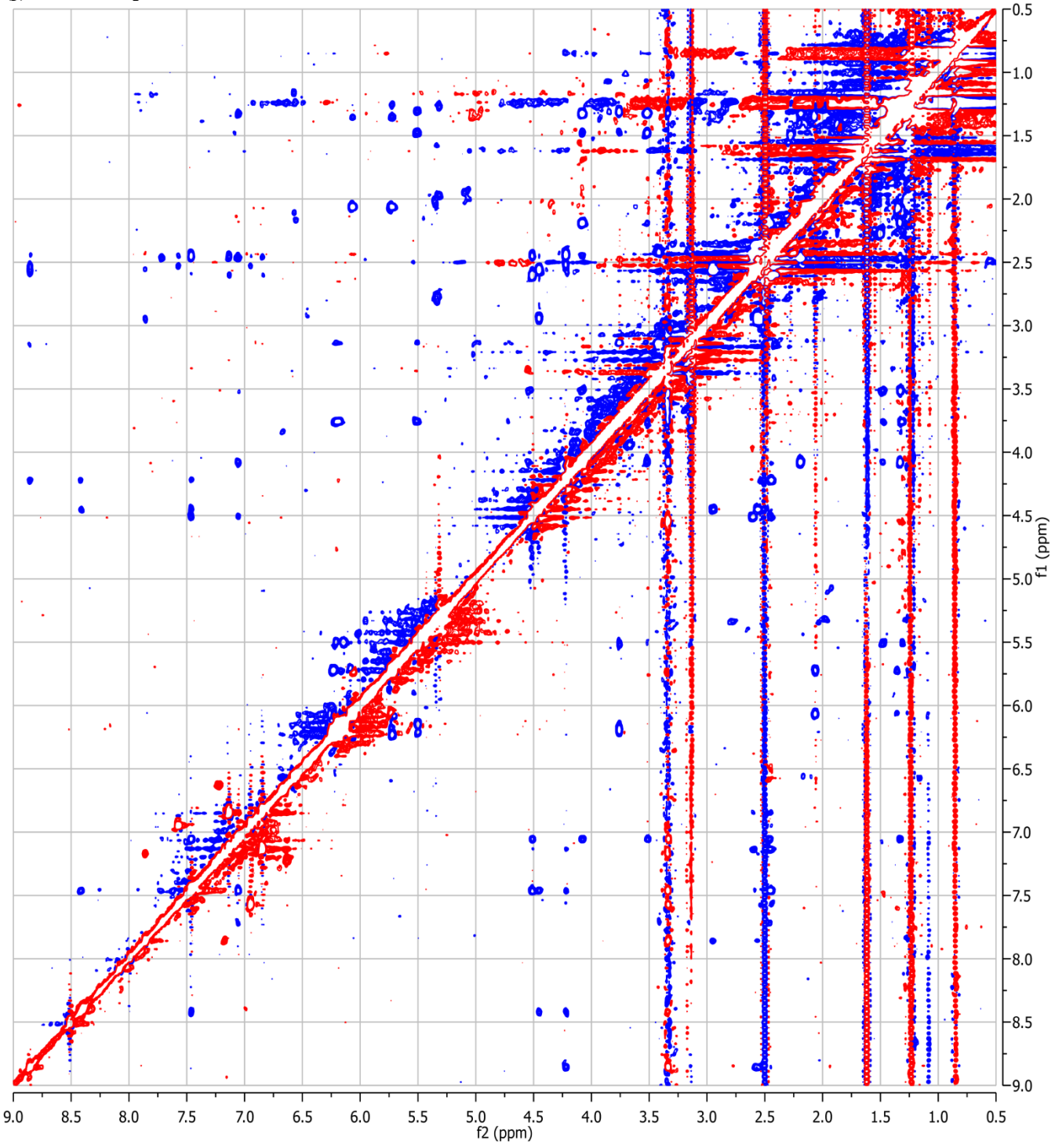

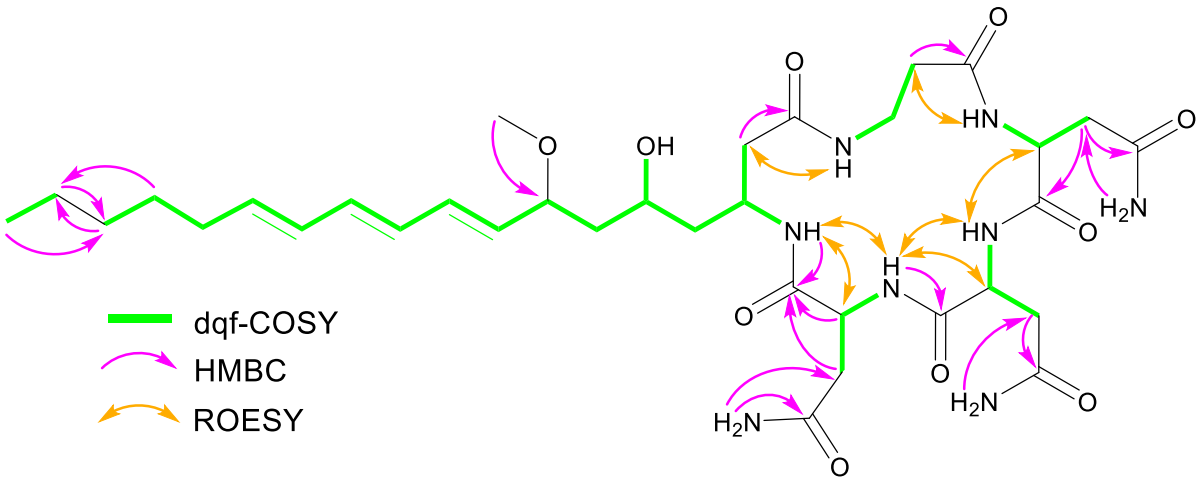

Supplementary Figure 4. Key dqf-COSY, HMBC, and ROESY correlations used to establish the molecular connectivity of nemamide A.

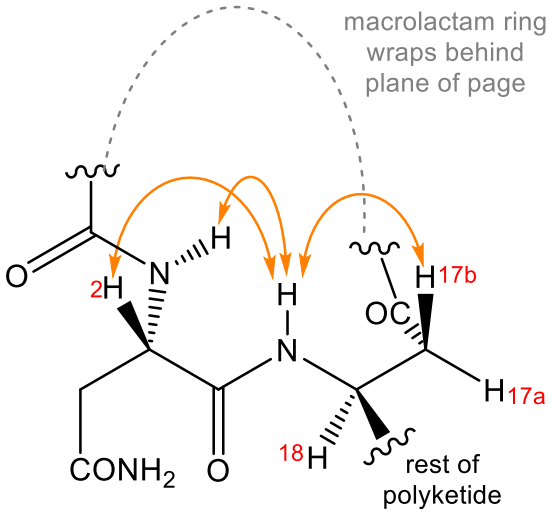

Supplementary Figure 5. Relative configuration of the stereocenters at C-2 and C-18. Nemamide A must have the absolute configuration shown (2*S*,18*R*) or the opposite absolute configuration (2*R*,18*S*) based on key ROESY correlations (indicated with orange double-headed arrows). The conformation depicted accounts for the weak *J* coupling between H-17a and 18 and the strong *J* coupling between H-17b and 18.

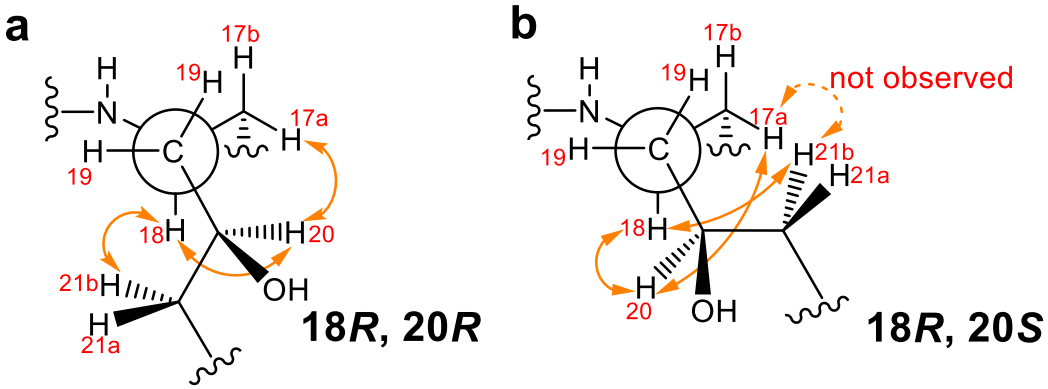

Supplementary Figure 6. Relative configuration of the stereocenters at C-18 and C-20. (**a**) Nemamide A has the absolute configuration shown (18*R*,20*R*) or the opposite absolute configuration (18*S*,20*S*) based on key ROESY correlations (indicated with orange double-headed arrows). The depicted conformation accounts for the weak *J* coupling between H-20 and H-21b and the strong *J* coupling between H-20 and H-21a. (**b**) The absolute configuration shown (18*R*,20*S*) or the opposite absolute configuration (18*S*,20*R*) is unlikely given the relative strength of the three ROESY correlations shown, as well as the fact that no correlation between H-17a and H-21b is observed in the ROESY spectrum.

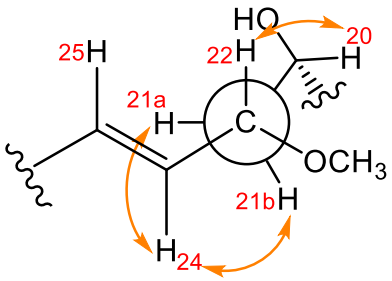

Supplementary Figure 7. Relative configuration of the stereocenters at C-20 and C-22. Nemamide A must have the absolute configuration shown (20*R*,22*S*) or the opposite absolute configuration (20*S*,22*R*) based on key ROESY correlations (indicated with orange double-headed arrows). The depicted conformation accounts for the weak *J* coupling between H-20 and H-21b and the strong *J* coupling between H-20 and H-21a. It also accounts for the weak *J* coupling between H-21a and H-22 and the strong *J* coupling between H-21b and H-22.

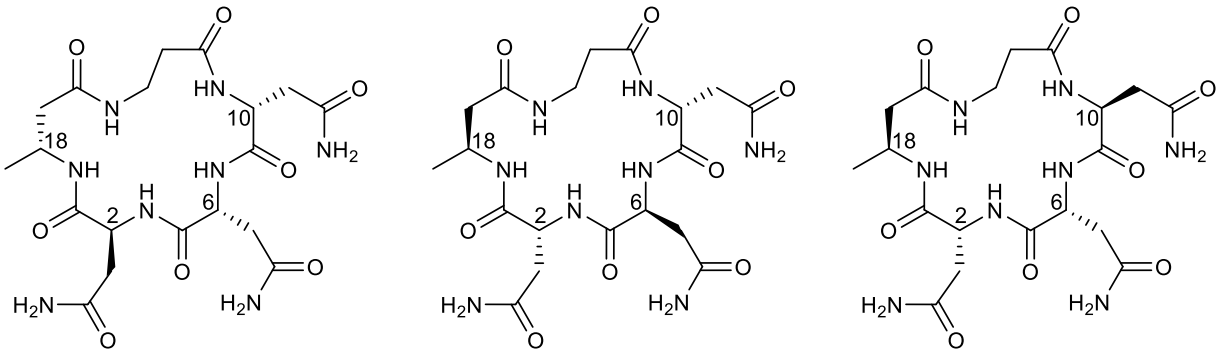

cyclic peptide **3** (2*S*,6*R*,10*R*,18*R*)

cyclic peptide **4** (2*R*,6*S*,10*R*,18*S*)

cyclic peptide **5** (2*R*,6*R*,10*S*,18*S*)

Supplementary Figure 8. Chemical structures of the model cyclic peptides that were synthesized in order to determine the absolute configurations of C-2, C-6, C-10, and C-18 in nemamide A. There are three possible positions for the L-Asn in the macrolactam ring of nemamide A, leading to the configurations 2*S*,6*R*,10*R*, 2*R*,6*S*,10*R*, and 2*R*,6*R*,10*S*. The relative configuration of the stereocenter at C-18 can be determined relative to the configuration of the most C-terminal Asn (that is, the configuration of the stereocenter at C-2), based on key ROESY correlations (Supplementary Fig. 5). Therefore, there are three possible absolute configurations for the four stereocenters in the macrolactam ring of nemamide A. Model cyclic peptides in which the polyketide tail of nemamide A was truncated as a methyl group were synthesized with the three possible absolute configurations of the four stereocenters: cyclic peptide **3** (2*S*,6*R*,10*R*,18*R*), cyclic peptide **4** (2*R*,6*S*,10*R*,18*S*), and cyclic peptide **5** (2*R*,6*R*,10*S*,18*S*).

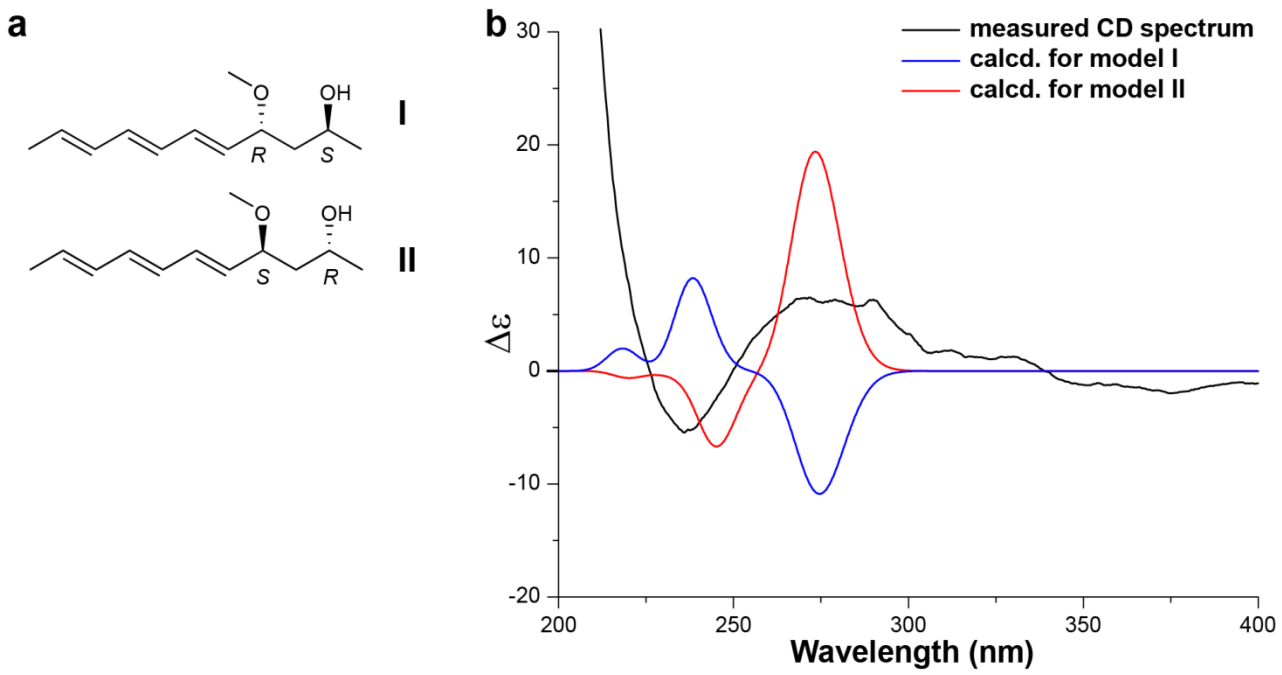

Supplementary Figure 9. Predicted and observed CD spectra of nemamide A. (**a**) Structures of model compounds I and II that were used to generate calculated CD spectra. In nemamide A, the configuration of the stereocenter at C-22 can be determined relative to the configuration of the stereocenter at C-20, based on key ROESY correlations (Supplementary Fig. 7). Thus, nemamide A is either 20*R*,22*S* or 20*S*,22*R*. The Cotton effects in the CD spectrum of nemamide A are predicted to depend largely on the configuration of the stereocenter nearest to the triene chromaphore (C-22). Thus, comparison of the calculated CD spectra of model compounds I and II to the CD spectrum of nemamide A should provide further confirmation of the absolute configuration of C-22 (and therefore C-20) in nemamide A.[3,4] (**b**) CD spectrum of nemamide A obtained in methanol, as well as calculated CD spectra of model compounds I (corresponding to nemamide A with 20*S*,22*R* configuration) and II (corresponding to nemamide A with 20*R*,22*S* configuration), suggesting that nemamide A has the 20*R*,22*S* configuration. The CD spectrum of nemamide A is weak because the compound has limited solubility in methanol and only dissolves well in dimethyl sulfoxide, which is not compatible with CD spectroscopy (of nemamide A). For calculating the CD spectra of the model compounds, the low energy conformations of the compounds were first calculated using Sybyl-X 2.1. Specifically, the random search algorithm was performed (100 cycles with an energy cutoff of 3.0 kcal/mol) while enforcing the constraints that the dihedral angles between "H-20" and "H-21a" and between "H-21b" and "H-22" should be 180° and that the distances between "H-20" and "H-22", "H-21a" and "H-24", and "H-21b" and "H-24" should be 0-3 Å (based on relevant coupling constants and ROESY correlations for Nemamide A; see Supplementary Table 1 and Supplementary Fig. 3). The CD spectra of the low energy conformers of the model compounds were then calculated using time dependent density functional theory (B3LYP functional/ 6-31G(d) basis set) with Gaussian 09. No UV shift correction was required. A sigma value of 0.16 eV was applied to the simulated CD spectra in SpecDis 1.60. The calculated CD spectra for the low energy conformers of each model compound were then Boltzmann-averaged.[3] The calculated CD spectra of the two model compounds are not exact mirror images because a defined (rather than infinite) number of low energy conformations were used to generate the Boltzmann-averaged CD spectrum.[5,6]

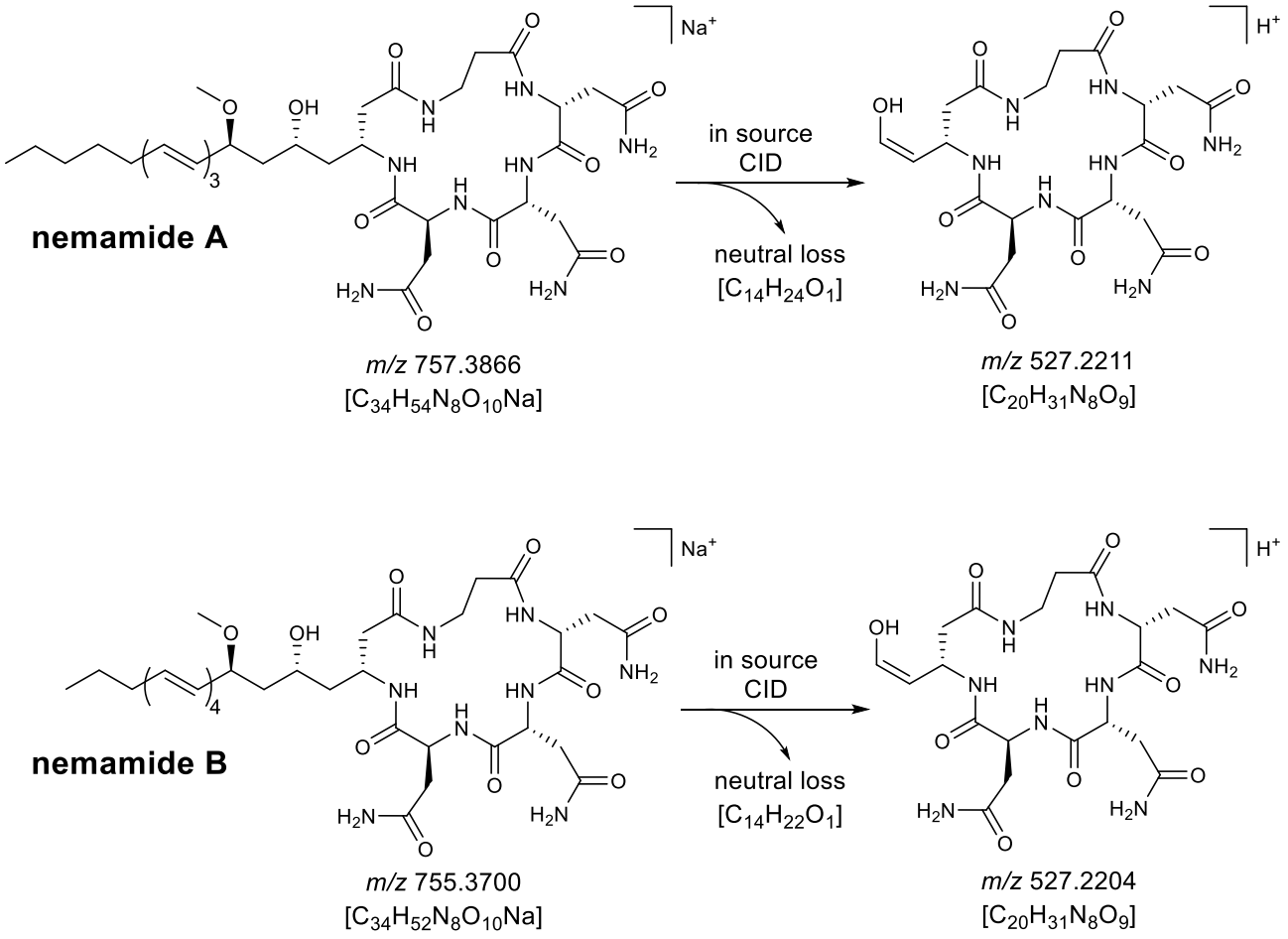

Supplementary Figure 10. In-source collision-induced dissociation (CID) of nemamide A and B. Both nemamide A and B undergo a neutral loss to yield the same product ion, indicating that the additional double bond in nemamide B is located in the neutral loss fragment.

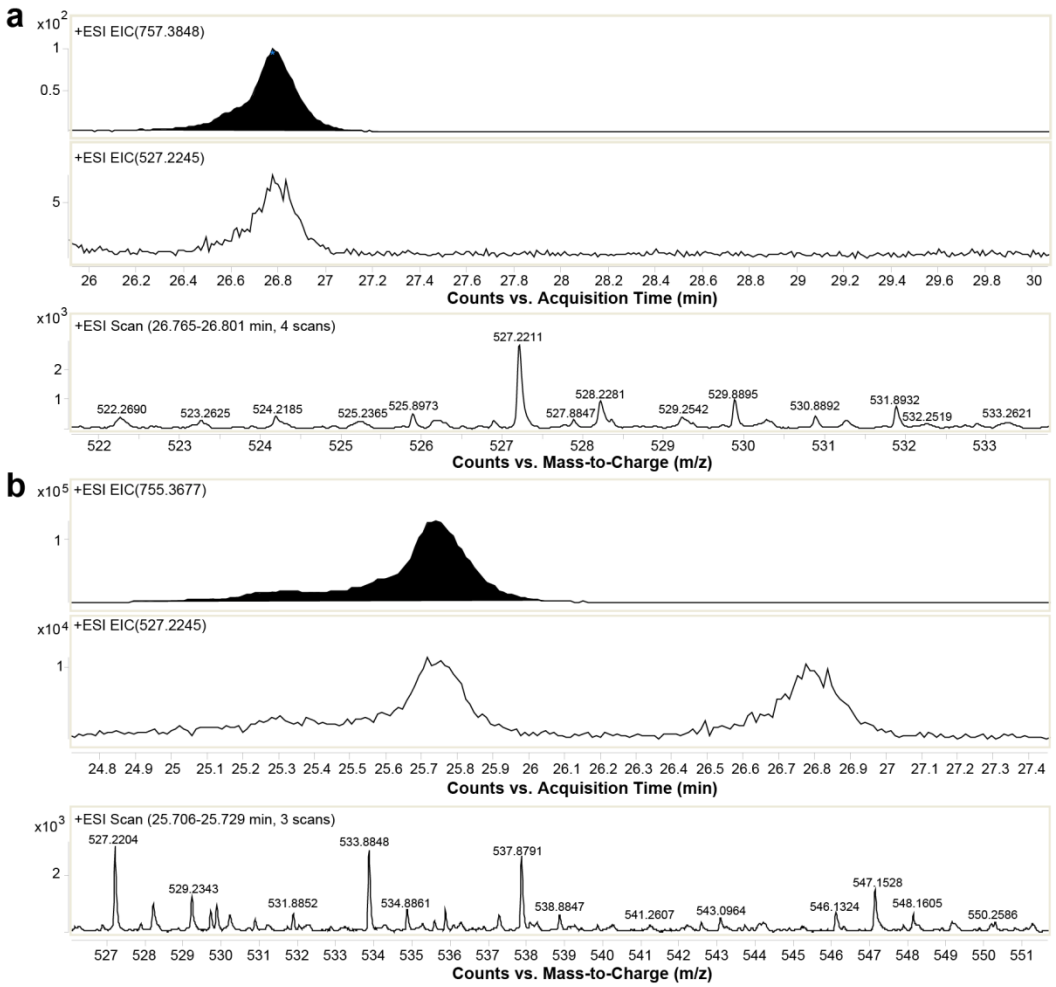

Supplementary Figure 11. High-resolution LC-MS data for in-source collision-induced dissociation (CID) of nemamide A and B. Raw data for nemamide A (**a**) and nemamide B (**b**) that serve as the basis for Supplementary Figure 10.

Supplementary Figure 12. NMR spectra for nemamide B in dimethyl sulfoxide-d_6.

(**a**) ^{1}H NMR spectrum (with water suppression, contaminant peaks are indicated with asterisks).

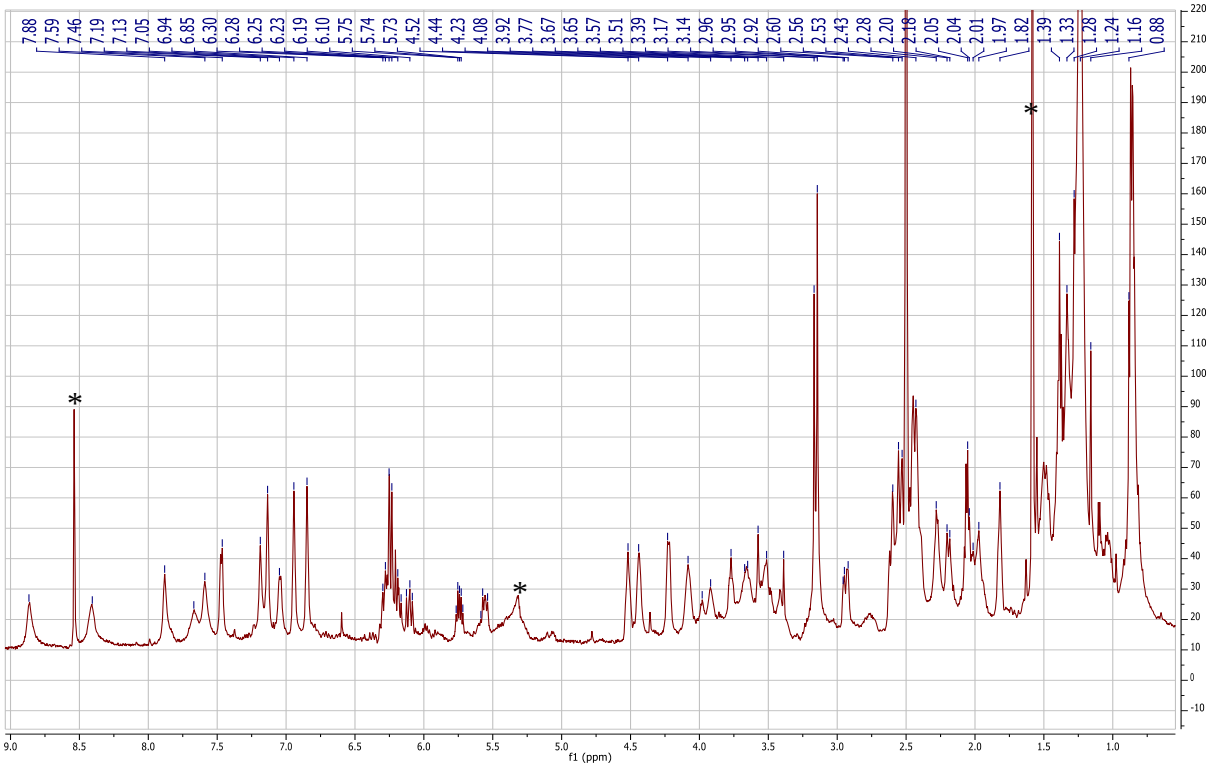

(**b**) ^{1}H NMR spectrum (without water suppression, contaminant peaks are indicated with asterisks).

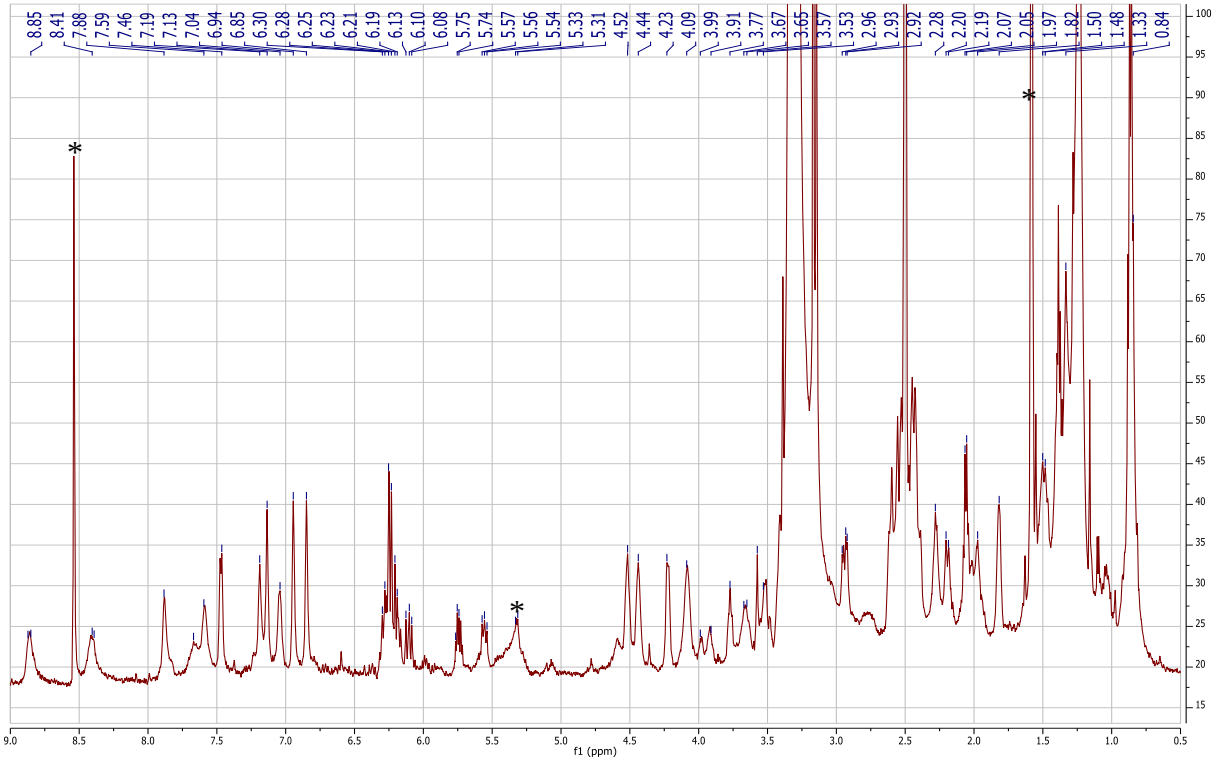

(**c**) dqf-COSY spectrum.

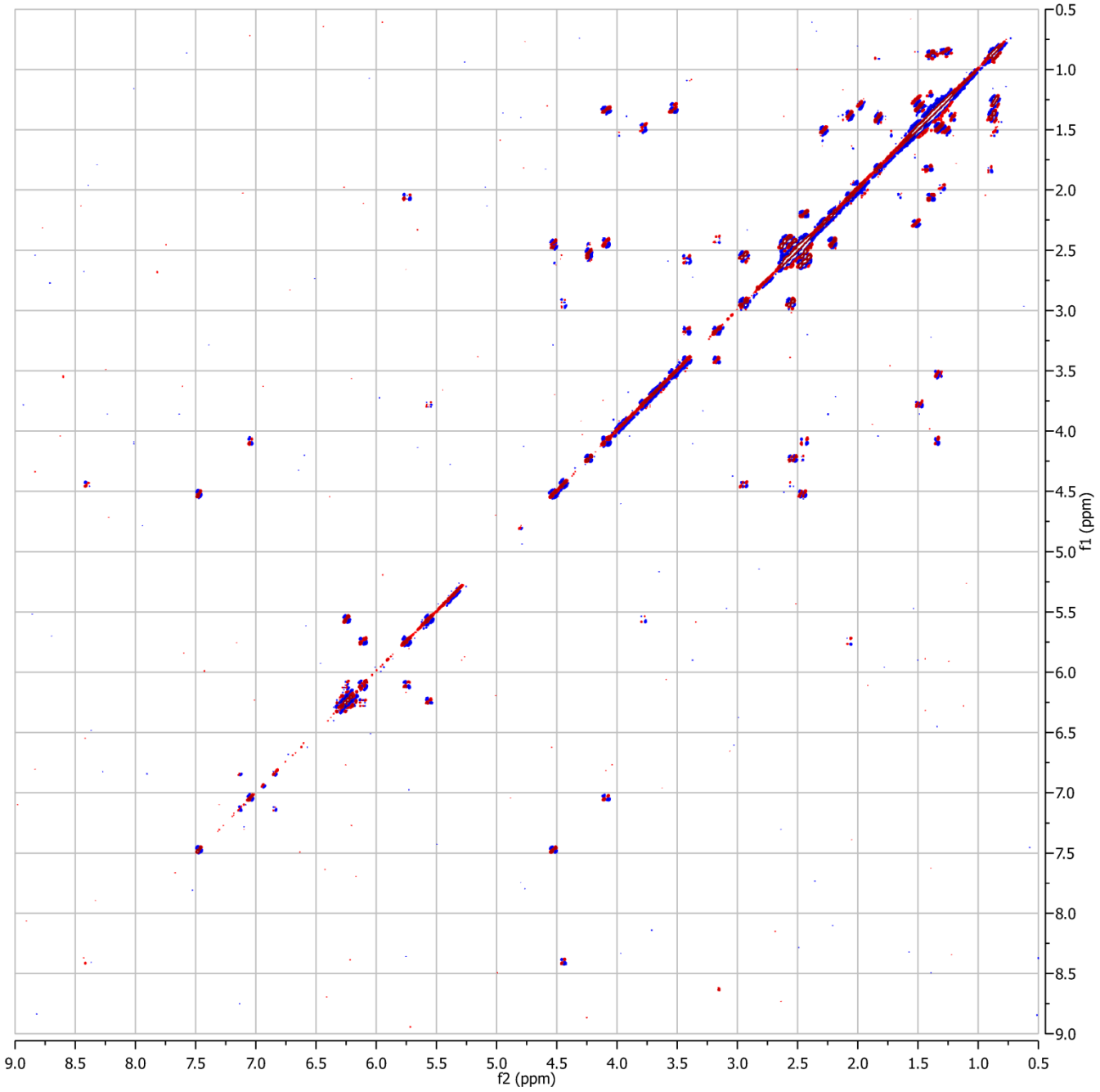

(**d**) dqf-COSY spectrum (0.5-5ppm region).

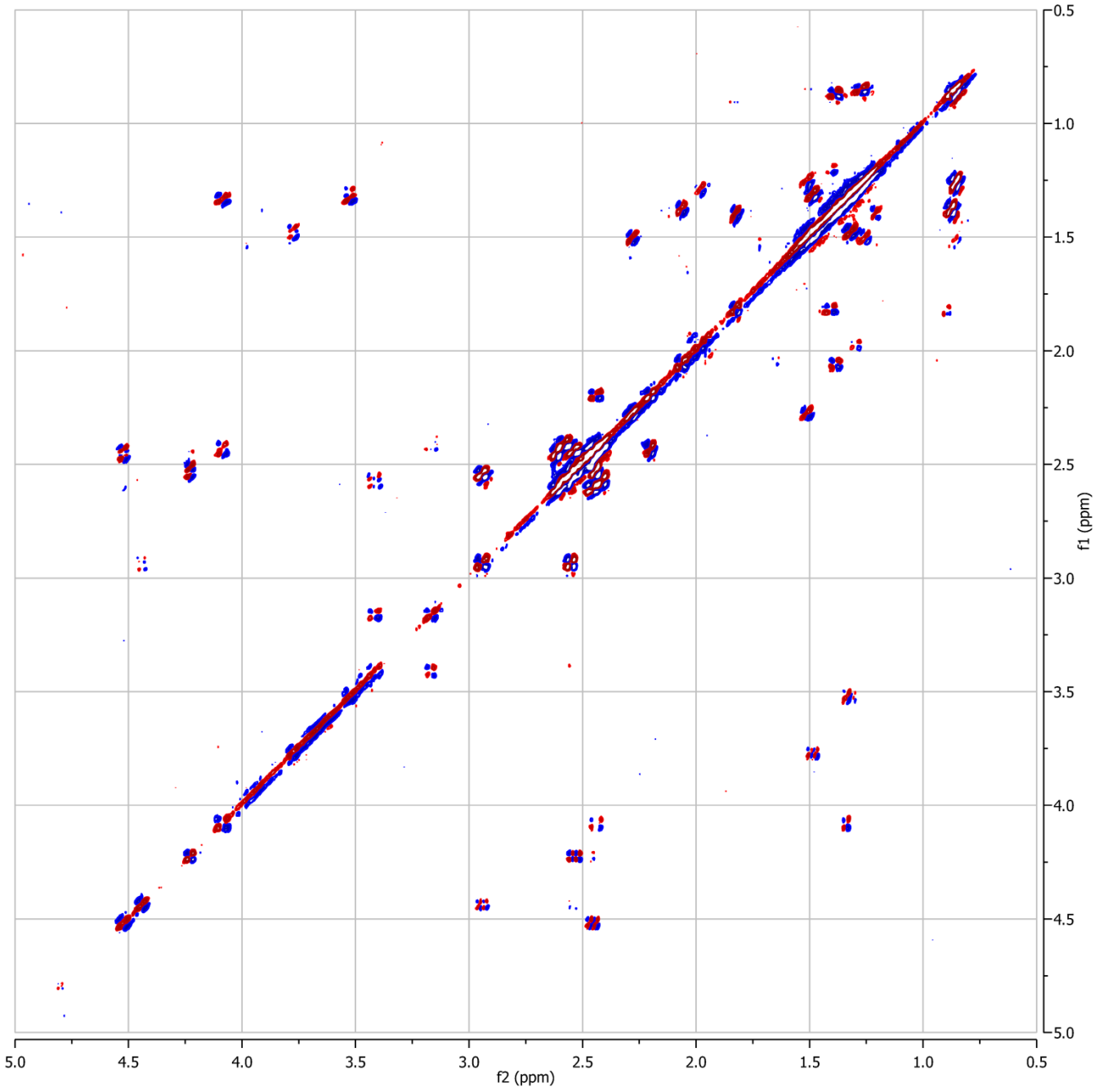

(**e**) TOCSY spectrum.

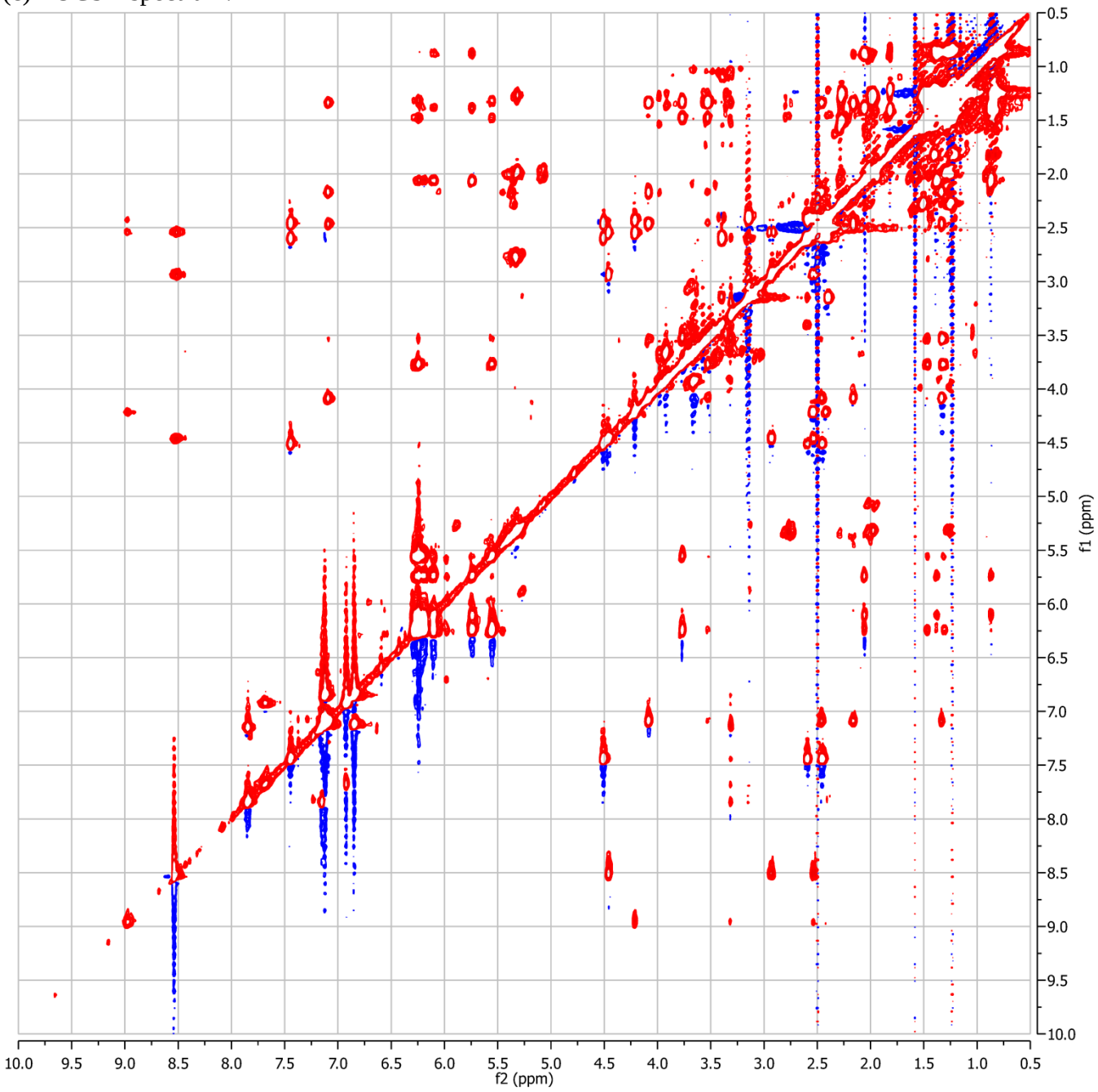

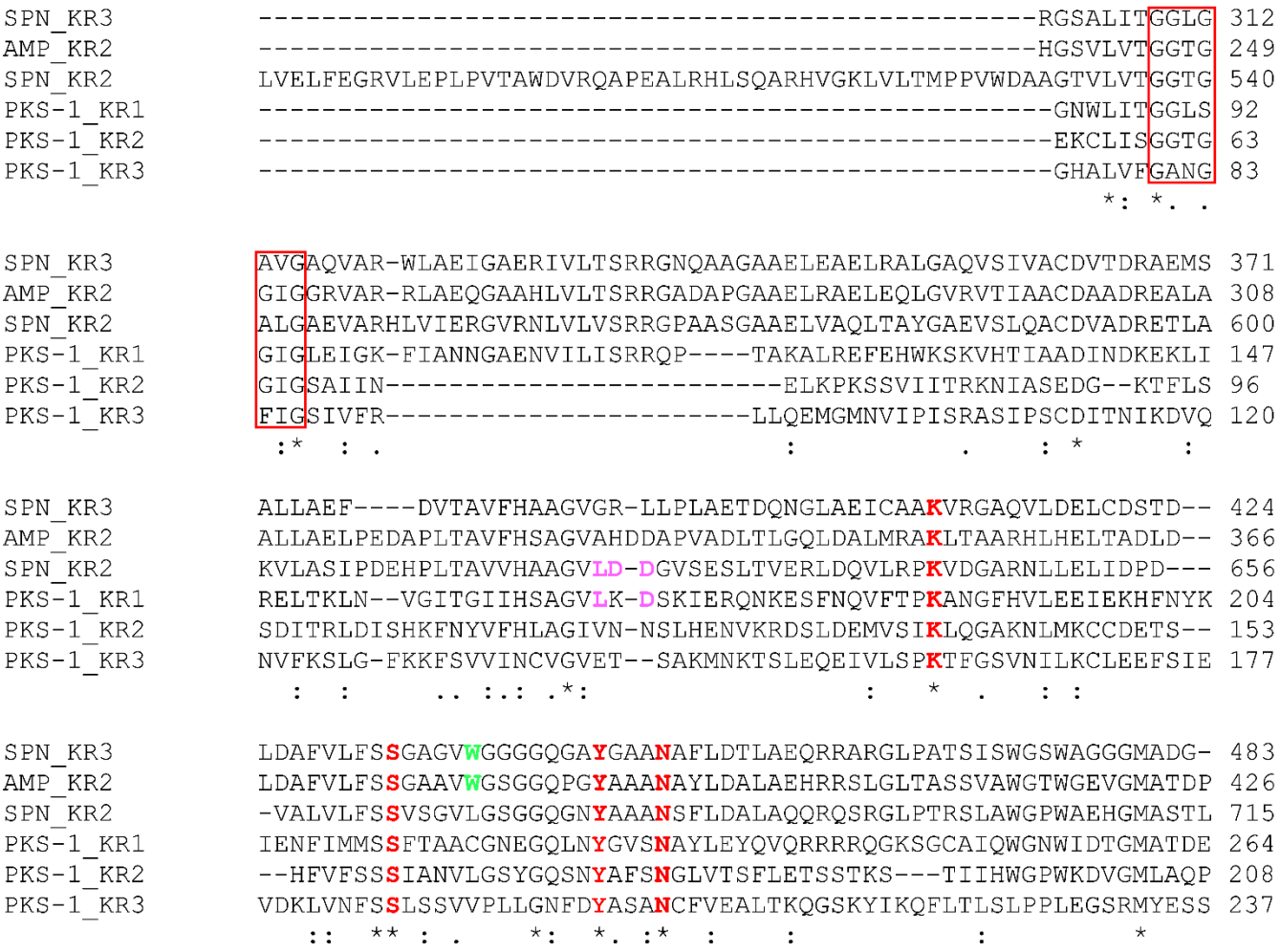

Supplementary Figure 13. Alignment of the PKS-1 KR domains with bacterial KR domains. The three ketoreductase (KR) domains in PKS-1 (KR_1, KR_2, and KR_3) were aligned with bacterial KR domains, SPN_KR3 and AMP_KR2 (A-type) and SPN_KR2 (B-type). Whereas A-type KR domains catalyze the formation of an L-configured alcohol at the 3-position relative to the thioester in the growing polyketide, B-type KR domains catalyze the formation of a D-configured alcohol at the 3 position relative to the thioester.[7] The PKS-1 KR_1 is a B-type KR domain, which provides further support for the assigned configuration at C-22 in nemamide A. Although PKS-1 KR_1 has an LKD motif instead of an LDD motif, the LKD sequence is seen in the chicken FAS KR domain, which is presumed to be a B-type KR domain.[8] PKS-1 KR_2 and KR_3 do not have characteristic residues of either an A-type or a B-type KR domain. Sequences were aligned with Clustal Omega.[9] KR domains are from spinosyn (Spn) and amphotericin (Amp) PKSs. Red boxes indicate possible NADP binding domains, red residues indicate catalytic residues, pink residues ("LDD") are characteristic of B-type KR domains, and green residues ("W") are characteristic of A-type KR domains.

```
PKS-1_TE     EIAAH---AGNKRIFVMGHSMGGIMSREIVAELK-IWGYDIPFVMLFDSWVLRTNELDIE    107
NRPS-1_TE    ESAEN---IETSKLVFIGASSAGTFAFSTSQLFA-DDD---VTVLLLDTG----------    274
SOR_P_TEI    TTLAC---ARNSPFVLFGHSSGGNIAHMVAEHLE-SIGHGPAGVVLLDSY----DYASPA    110
AMP_P_TEI    SVLMA---SDGEPFVMVGHSTGGSLAYLAAGVLEDTWGVKPEAVVLLDTASIRYNPSEGN    114
SPN_P_TEI    AVLQE---FAGGSFVLVGHSSGGWLAHEVAGELE-RRGVVPAGVVLLDTY----IPGEIT    109
SPI_P_TEI    AIVRS---TAGSPFAIVAYSSSGWLAYATASCLE-SKGSSPRALVLLDHV----DQ----    104
AVE_P_TEI    AIVRF---TDGAPFALAGHSAGGWFVYAVTSHLE-RLGVRPEAVVTMDAY----LPDDGI    110
PIK_P_TEI    AILRA---AGDAPVVLLGHSGGALLAHELAFRLERAHGAPPAGIVLVDPY----PPGHQE    115
ERY_P_TEI    AVIRT---QGDKPFVVAGHSAGALMAYALATELL-DRGHPPRGVVLIDVY----PPGHQD    109
BAC_N_TEI    IIKNI---QGEGPYTLIGYSSGGILAFDVAKELN-RQGYEVEDLIIIDSK----YRTKAE    97
TYR_N_TEI    AITAI---DPSGPYTLMGYSSGGNLAFEVAKELE-ERGYGVTDIILFDSY----WKDKAI    97
SUR_N_TEI    LIQKL---QPEGPLTLFGYSAGCSLAFEAAKKLE-GQGRIVQRIIMVDSY----KKQGVS    114
MYX_PN_TEI   EVRKV---RPKGPYRLGGWSTGGILAQAMARQLE-EAGEQVELLMLLETW----SPTVYQ    104
HEC_PN_TEI   AIKSV---QPKGPYLLGGHSFGGLVAFETAQQLQ-KQGDEVAKLFIIDMR----APAVDK    108
TUB_PN_TEI   ELREL---QPRGPYRLGGWSFGCVVAYEVALQLE-AAGEQVALLSLLDFP----APSGQR    108
CHO_PN_TEI   AIQQI---QPSGPYHLGGHSAGARIAFAVALELQ-RRGAEVPLVSIVDMR----PPGRGA    105
MEG_P_TEII   VLRDL---VGEVPFALFGHSMGALVAYETARRLEARPGVRPLRLFVSGQT----APRVHE    126
PIK_P_TEII   ATEPW---WQEGRLAFFGHSLGASVAFETARILEQRHGVRPEGLYVSGRR----APSLAP    135
BOR_P_TEII   VLRA----RVHQPVALFGHSMGATLAFELARRFESAGIS-LEALLVSARP----APSRQR    131
TYL_P_TEII   ELRRLLDAPDGVPVALFGHSMGAVVAYETARLLHRSGAPRPAGLILSGRR----APTADR    151
KEN_P_TEII   ALGA---RSDGRPFALFGHSMGSLVAFETARRLQTRGA-APSVLFASGRP----APSCLR    128
RIF_P_TEII   VLRP----FGDRPLALFGHSMGAIIGYELALRMPEAGLPAPVHLFASGRR----APSRYR    130
BAC_N_TEII   QVQAE---RKGDDYALFGHSMGSLLAYELYYQMSGAGAEKPVHIFFSGYK----APNRIR    111
MIC_N_TEII   AILP----HLTKPFAFFGHSMGGLVSFELARLLRKEYNQSPLHLFVSGYR----APQIPD    138
```

Supplementary Figure 14. Alignment of PKS-1 and NRPS-1 TE domains with bacterial TE domains. The PKS-1 and NRPS-1 TE domains were aligned with bacterial TEI and TEII domains. TEI domains cleave polyketides/nonribosomal peptides from PKS/NRPSs once biosynthesis is complete, while TEII domains have editing functions.[10] Both the PKS-1 TE domain and the NRPS-1 TE domain have the Ser-Asp-His catalytic triad of TEI domains. Red residues indicate catalytic residues (portion of sequence alignment showing conserved His is not shown). Although the PKS-1 TE domain appears to be most similar to PKS-NRPS TEI domains (see Supplementary Fig. 15), it does have the sequence motif around the catalytic Ser (GHSMG) that is characteristic of TEII domains. Sequences were aligned with Clustal Omega.[9] TE domains are from the PKS (P), NRPS (N), and PKS-NRPS (PN) assembly lines that biosynthesize soraphen (Sor), amphotericin (Amp), spinosyn (Spn), spirangien (Spi), avermectin (Ave), pikromycin (Pik), erythromycin (Ery), bacitracin (Bac), tyrocidine (Tyr), surfactin (Sur), myxothiazol (Myx), hectochlorin (Hec), tubulysin (Tub), chondramid (Cho), megalomicin (Meg), borrelidin (Bor), tylosin (Tyl), kendomycin (Ken), rifampicin (Rif), and microcystein (Mic).

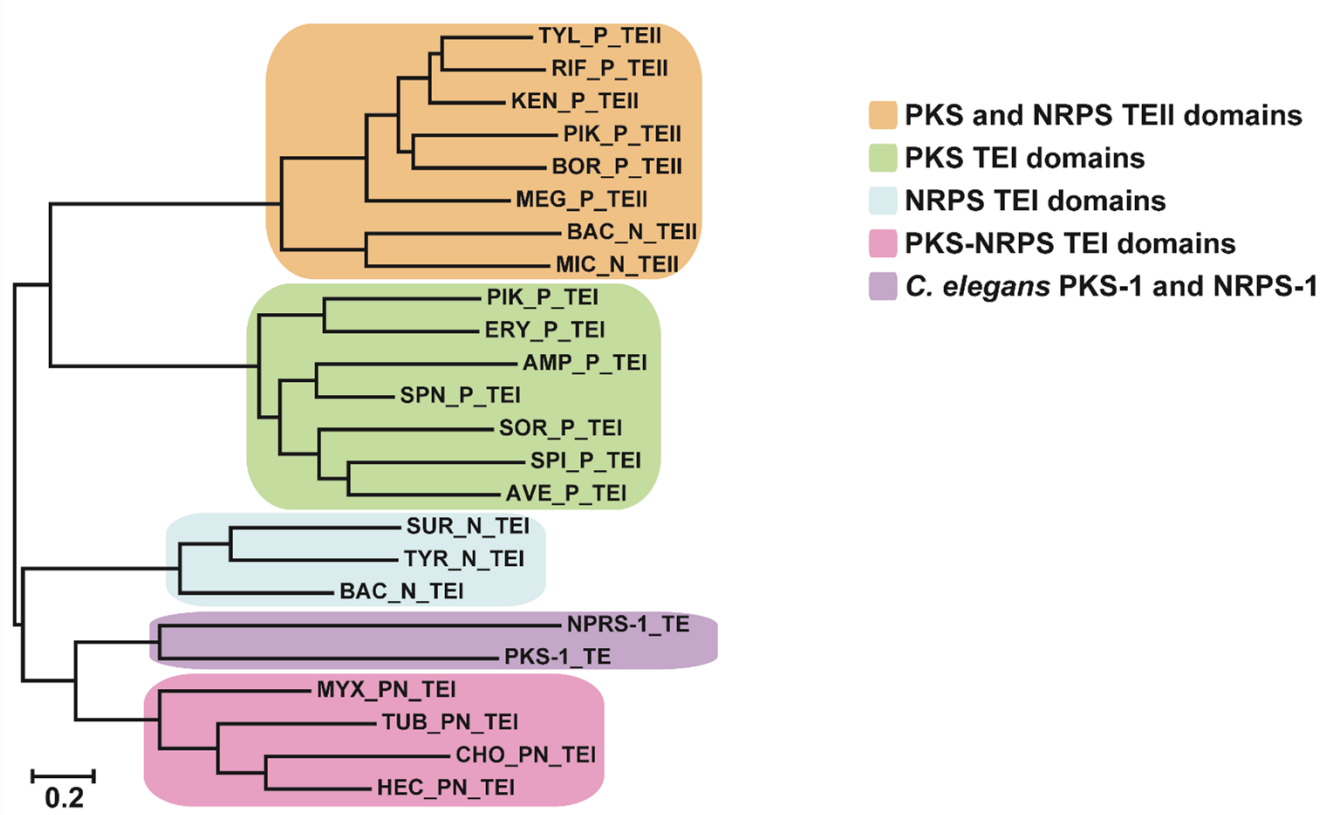

Supplementary Figure 15. Phylogeny of the PKS-1 and NRPS-1 TE domains and bacterial TE domains. Both the PKS-1 and NRPS-1 TE domains cluster with the TEI domains of bacterial hybrid PKS-NRPSs. TE domains are described in Supplementary Figure 14. Phylogenetic tree was generated in MEGA 6.[11]

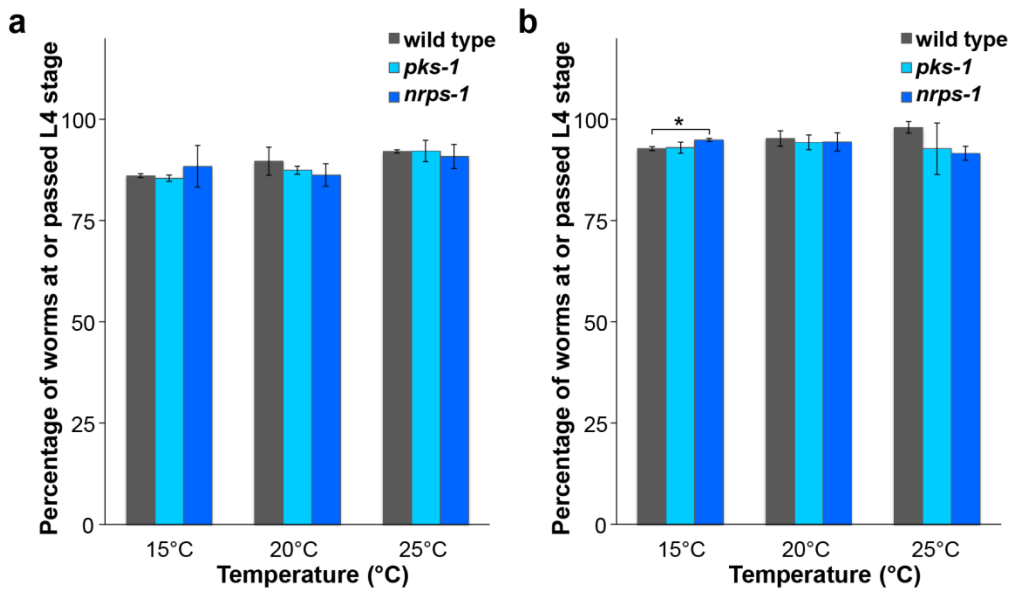

Supplementary Figure 16. Comparison of development of wild-type, *pks-1*, and *nrps-1* worms. (**a**) Development of eggs (obtained through alkaline-bleach treatment of gravid adults) to the L4 stage for wild-type, *pks-1*, and *nrps-1* worms at different temperatures. Eggs were obtained using a similar method as in Figure 2c, but were hatched in food such that they did not go through L1 arrest. The lack of difference between wild type and mutants suggests that the delayed L1 recovery of the mutants seen in **Figure 2c** is not due to the alkaline-bleach treatment or to a general delay in developmental rate. (**b**) Development of eggs (obtained by allowing gravid adults to lay eggs) to the L4 stage for wild-type, *pks-1*, and *nrps-1* worms at different temperatures. The lack of difference between wild type and mutants suggests that the delayed L1 recovery of the mutants seen in **Figure 2c** is not due to a general delay in developmental rate. Data represent the mean ± SD of two independent experiments. Two-tailed, unpaired t-tests were used to determine statistical significance. All *P* values were non-significant except as indicated (*$P \leq 0.05$).

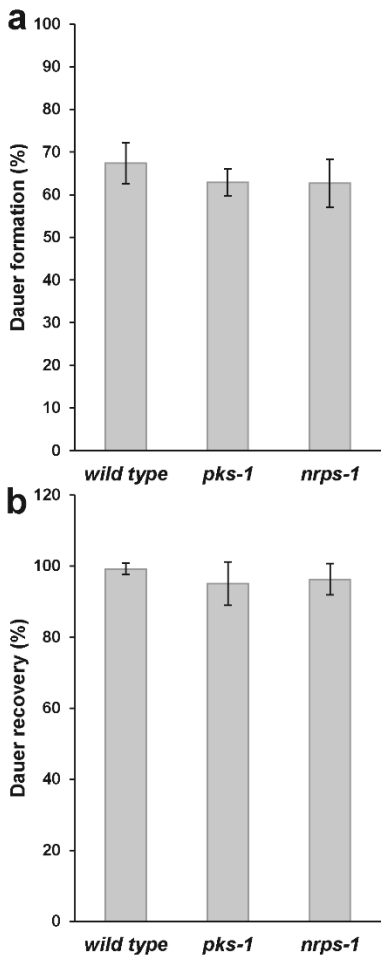

Supplementary Figure 17. Dauer formation and recovery in wild-type, *pks-1*, and *nrps-1* worms. (**a**) Dauer formation in wild-type, *pks-1*, and *nrps-1* worms exposed to 1 μM asc-C6-MK (ascr#2) in the dauer formation assay at 25 °C. (**b**) Recovery of wild-type, *pks-1*, and *nrps-1* dauers after being placed on a lawn of OP50 bacteria for 24h at 20 °C. Data represent the mean ± SD of two (**a**) or four (**b**) independent experiments. In (**a**) and (**b**), two-tailed, unpaired t-tests showed that there is no significant difference between the wild type and mutants.

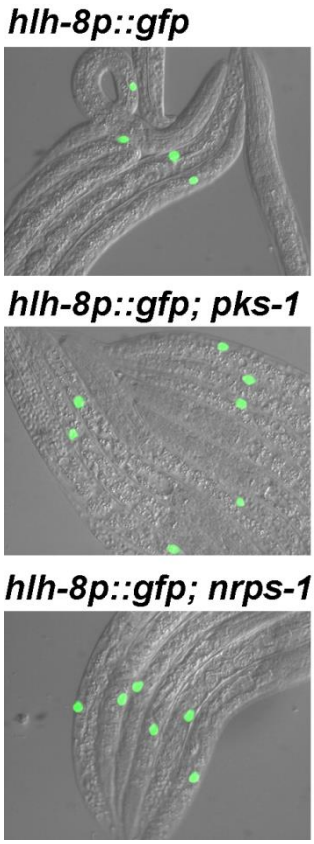

Supplementary Figure 18. M-cell imaging in wild-type, *pks-1* and *nrps-1* backgrounds. Fluorescence images showing that the M-cell (identified using the M-cell-specific reporter, *hlh-8p:gfp*) does not divide during L1 arrest in wild-type, *pks-1*, and *nrps-1* worms. M-cell arrest in arrested L1s is an indication that the worm has properly arrested somatic progenitor cell division during starvation. Certain mutants in the insulin/IGF-1 pathway, such as *daf-16/foxo*, undergo improper M-cell division during L1 arrest.[12,13]

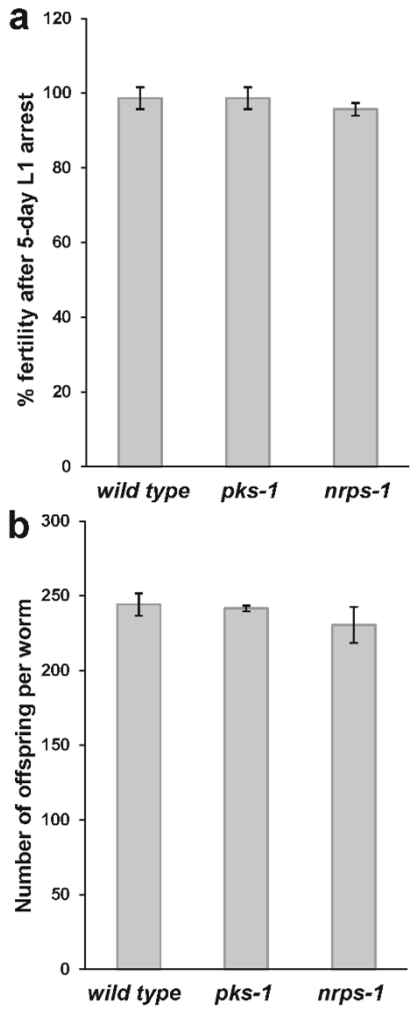

Supplementary Figure 19. Fertility and brood size in wild-type, *pks-1* and *nrps-1* worms that experienced extended L1 arrest. Percent fertility (**a**) and brood size (**b**) after L1s were subjected to five days of L1 arrest and then allowed to recover and develop into adults on food. The absence of fertility defects in the mutants suggests that the mutants maintain proper germline arrest during starvation-induced L1 arrest. Certain mutants in the insulin/IGF-1 pathway, such as *daf-18/pten*, undergo improper germline proliferation during L1 arrest, leading to fertility defects once the L1 recover and develop to the adult stage.[14,15] Data represent the mean ± SD of five independent experiments (n = 30) (**a**) or two independent experiments (n = 20) (**b**). In (**a**) and (**b**), two-tailed, unpaired t-tests showed that there is no significant difference between the wild type and the mutants.

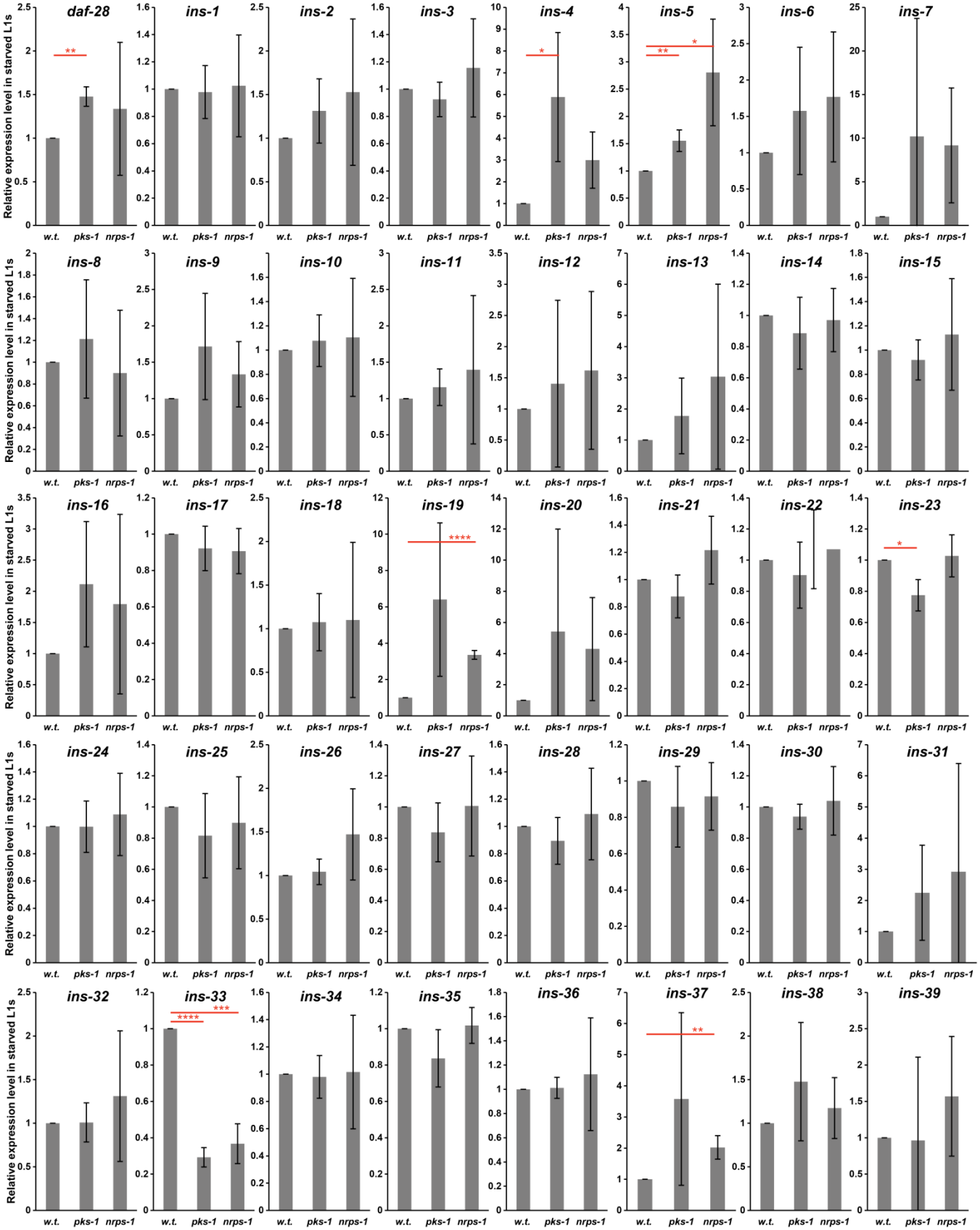
daf-28
ins-1
ins-2
ins-3
ins-4
ins-5
ins-6
ins-7
ins-8
ins-9
ins-10
ins-11
ins-12
ins-13
ins-14
ins-15
ins-16
ins-17
ins-18
ins-19
ins-20
ins-21
ins-22
ins-23
ins-24
ins-25
ins-26
ins-27
ins-28
ins-29
ins-30
ins-31
ins-32
ins-33
ins-34
ins-35
ins-36
ins-37
ins-38
ins-39
Relative expression level in starved L1s
w.t.
pks-1
nrps-1

Supplementary Figure 20. Expression of insulins in wild-type, *pks-1*, and *nrps-1* arrested L1s relative to wild-type arrested L1s, as determined by qRT-PCR. *ins-4*, *ins-5*, *ins-19*, and *ins-37* are expressed at higher levels in *pks-1* and/or *nrps-1* arrested L1s than in wild-type arrested L1s. *daf-28* is also expressed at higher levels in *pks-1* arrested L1s than in wild-type arrested L1s. Conversely, *ins-33* is expressed at lower levels in *pks-1* and *nrps-1* arrested L1s than in wild-type arrested L1s. Higher levels of expression of *ins-4* and *daf-28* in arrested L1s have been associated with reduced L1 arrest survival, and deletion of *ins-4* and *daf-28* has been associated with increased L1 arrest survival.[16] Data represent the mean ± SD of three independent experiments. Two-tailed, unpaired t-tests were used to determine statistical significance (*$P \leq 0.05$, **$P \leq 0.01$, ***$P \leq 0.001$, ****$P \leq 0.0001$).

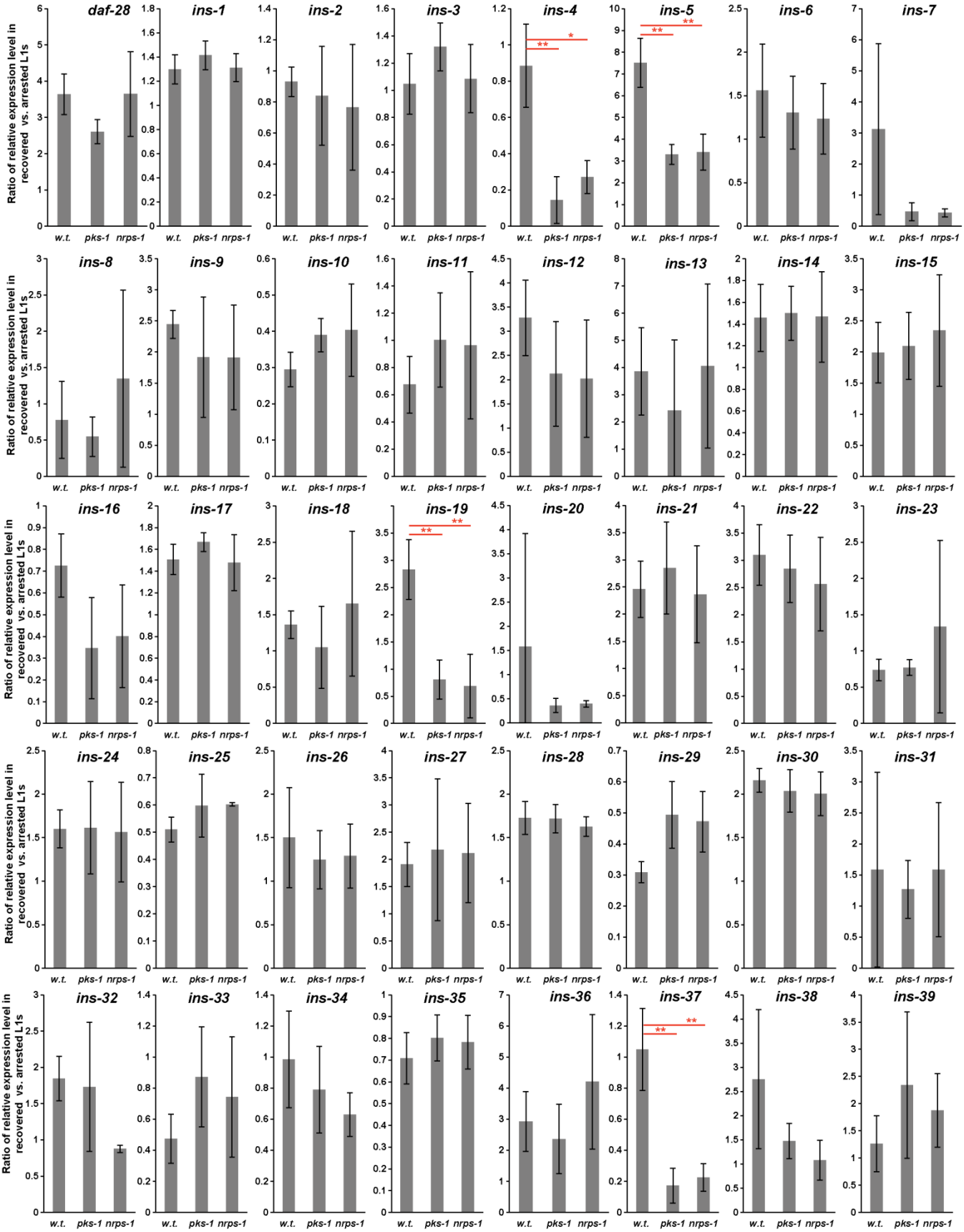
daf-28
ins-1
ins-2
ins-3
ins-4
ins-5
ins-6
ins-7
ins-8
ins-9
ins-10
ins-11
ins-12
ins-13
ins-14
ins-15
ins-16
ins-17
ins-18
ins-19
ins-20
ins-21
ins-22
ins-23
ins-24
ins-25
ins-26
ins-27
ins-28
ins-29
ins-30
ins-31
ins-32
ins-33
ins-34
ins-35
ins-36
ins-37
ins-38
ins-39
Ratio of relative expression level in recovered vs. arrested L1s
w.t.
pks-1
nrps-1
pks-1 nrps-1
*
**

Supplementary Figure 21. Expression of insulins in recovered versus arrested wild-type, *pks-1*, and *nrps-1* L1s, as determined by qRT-PCR. *ins-5* and *ins-19* are induced during recovery in wild-type L1s, but not induced (or not induced as much) in *pks-1* and *nrps-1* L1s. *ins-4* and *ins-37* are not induced during recovery (at least not at 6h post-recovery) in wild-type L1s, but are down-regulated in *pks-1* and *nrps-1* L1s. Data represent the mean ± SD of three independent experiments. Two-tailed, unpaired t-tests were used to determine statistical significance (*$P \leq 0.05$, **$P \leq 0.01$, ***$P \leq 0.001$, ****$P \leq 0.0001$).

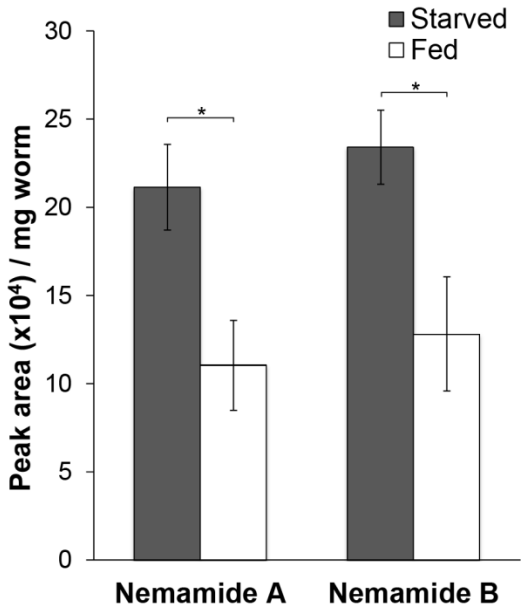

Supplementary Figure 22. Nemamide production in arrested and recovered L1s. Levels of nemamides A and B in arrested L1s and recovered L1s (6 h after addition of food). Data represent the mean ± SD of four independent experiments. Two-tailed, unpaired t-tests were used to determine statistical significance (*$P \leq 0.05$).

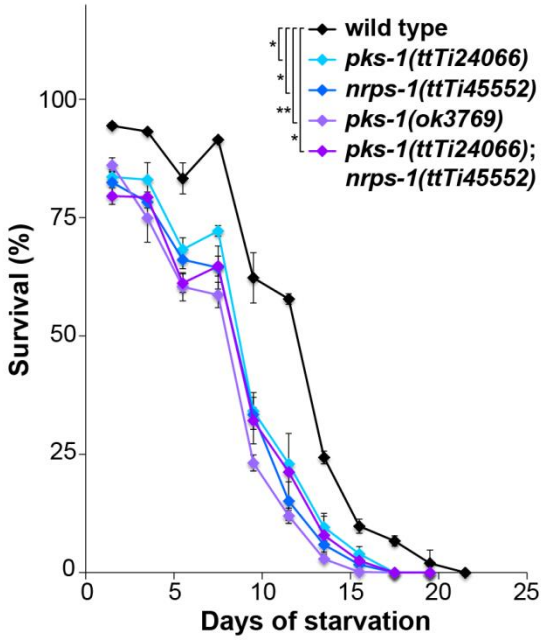

Supplementary Figure 23. L1 survival for wild-type and different mutant strains. In addition to the *pks-1(ttTi24066)* and *nrps-1(ttTi45552)* strains (which were the *pks-1* and *nrps-1* alleles used throughout this manuscript), we also tested L1 survival in the *pks-1(ok3769)* strain and the *pks-1(ttTi24066)*; *nrps-1(ttTi45552)* double mutant strain and obtained similar results. That is, no statistically significant difference was found for any of the tested mutants in terms of mean survival. The mean ± SD of three independent experiments are plotted. Mean survival (days ± SE) was calculated as described in Methods: 12.2±0.3 for wild type, 9.4±0.4 for *pks-1(ttTi24066)*, 8.9±0.4 for *nrps-1(ttTi45552)*, 7.7±0.4 for *pks-1(ok3769)*, and 8.7±0.5 for *pks-1(ttTi24066)*; *nrps-1(ttTi45552)*. A two-tailed, unpaired t-test was used to determine statistical significance (*$P \leq 0.05$, **$P \leq 0.01$, ***$P \leq 0.001$).

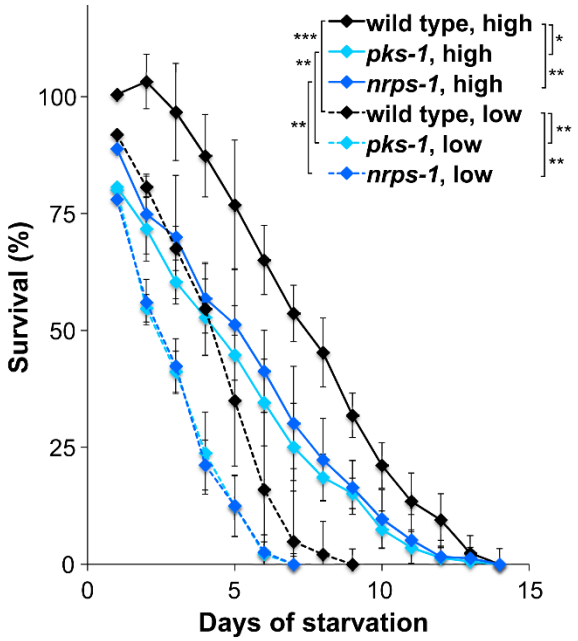

Supplementary Figure 24. L1 survival for wild-type, *pks-1*, and *nrps-1* worms at low and high population densities. Survival assays were performed at 25 °C. The mean ± SD of three independent experiments are plotted. Mean survival (days ± SE) was calculated as described in Methods: 8.3±0.2 for wild type/high, 6.4±0.4 for *pks-1*/high, 5.9±0.4 for *nrps-1*/high, 5.2±0.3 for wild type/low, 2.8±0.4 for *pks-1*/low, and 2.9±0.4 for *nrps-1*/low. A two-tailed, unpaired t-test was used to determine statistical significance (*$P \leq 0.05$, **$P \leq 0.01$, ***$P \leq 0.001$).

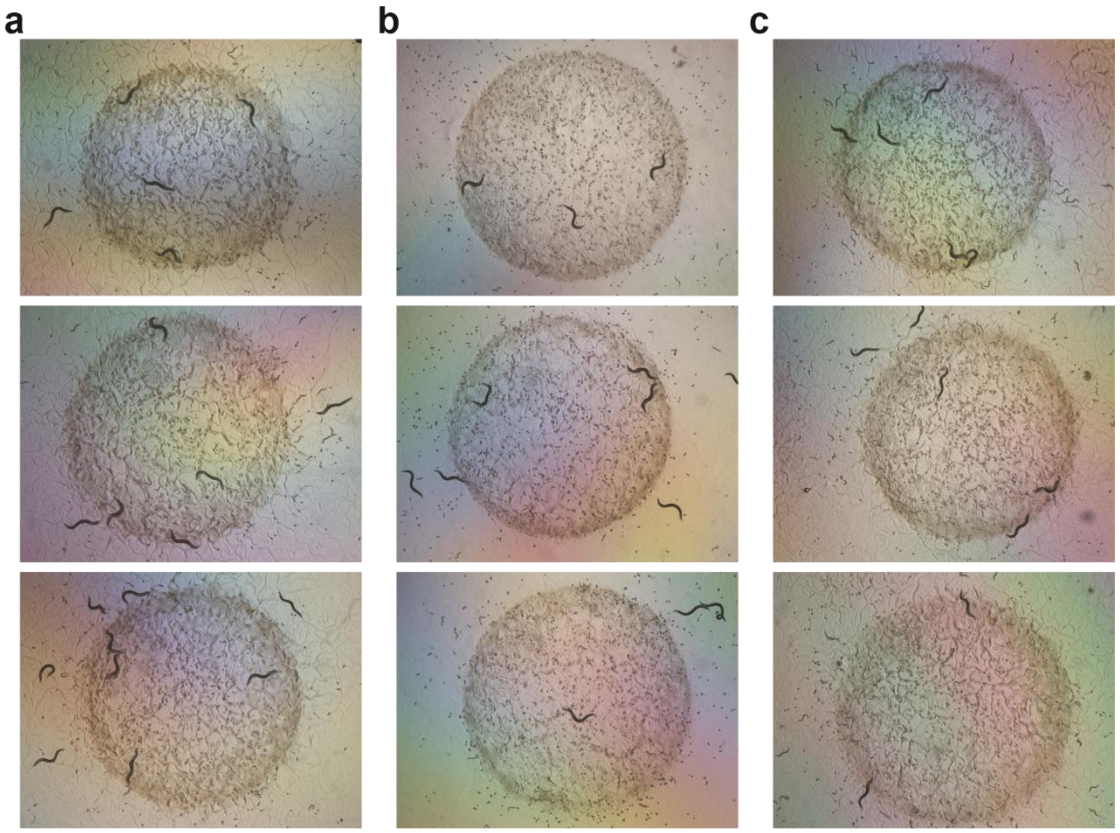

Supplementary Figure 25. Feeding rate of wild-type, *pks-1*, and *nrps-1* worms. Ten wild-type, *pks-1*, or *nrps-1* worms at the L4 stage were transferred to NGM-agar plates (containing 50 μM of 5-fluoro-2'-dexoxyuridine to prevent egg development) with a lawn of OP50 bacteria. The plates were incubated at 20 °C. The rate that the bacterial lawn was consumed was monitored over time, and no differences between the worms strains were observed. Photos of the plates with the wild-type (**a**), *pks-1* (**b**), and *nrps-1* (**c**) worms were taken after 6 d. Three replicates were done for each strain.

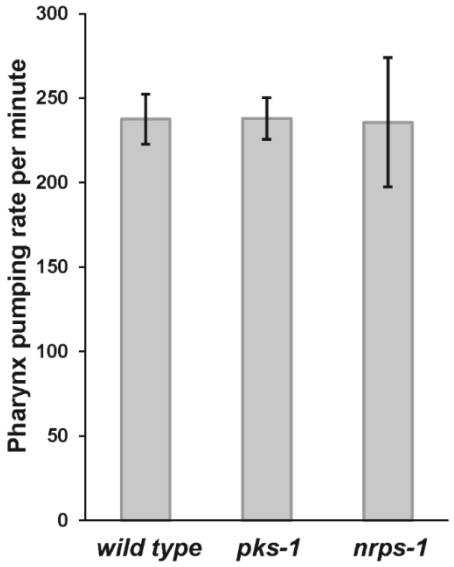

Supplementary Figure 26. Pharynx pumping rate of wild-type, *pks-1*, and *nrps-1* worms. Data represent the mean ± SD of two independent experiments. Two-tailed, unpaired t-tests showed that there is no significant difference between the wild type and the mutants.

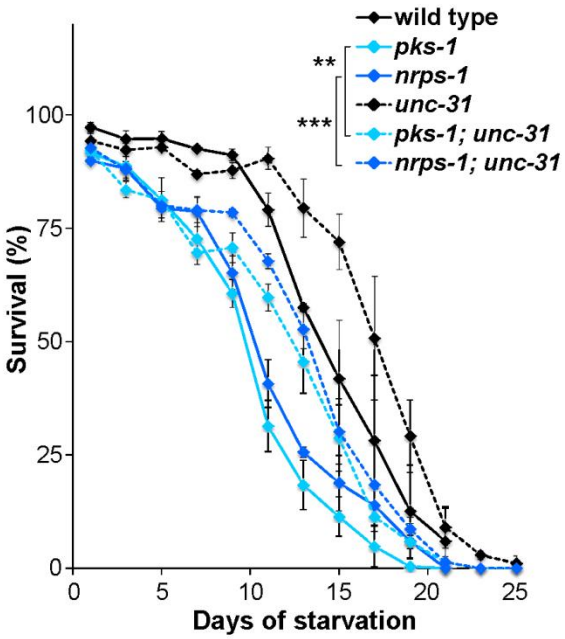

Supplementary Figure 27. Effect of an *unc-31(e928 null)* mutation on survival of arrested L1s. UNC-31 regulates insulin secretion and acts upstream of the insulin/IGF-1 pathway, which controls L1 survival in a manner dependent on the *daf-16/foxo* transcription factor.[12,17,18] The *unc-31(e928 null)* mutation was able to suppress significantly, but not completely, the reduced survival of the *pks-1* and *nrps-1* mutants. Thus, the nemamides likely extend L1 survival by negatively regulating UNC-31-mediated insulin signaling and UNC-31-independent pathways. Survival assays were performed at 20°C. Mean survival (days ± SE) was calculated as described in Methods: 14.3 ± 0.2 for wild type, 10.0 ± 0.2 for *pks-1*, 10.9 ± 0.2 for *nrps-1*, 17.5 ± 0.2 for *unc-31*, 13.1 ± 0.3 for *pks-1; unc-31*, and 13.9 ± 0.2 for *nrps-1; unc-31*. Data represent the mean ± SD of three independent experiments. A two-tailed, unpaired t-test was used to determine statistical significance (*$P \leq 0.05$, **$P \leq 0.01$, ***$P \leq 0.001$).

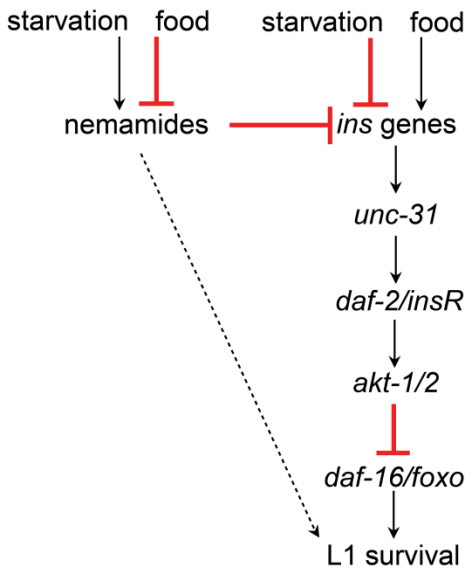

Supplementary Figure 28. Model for the role of the nemamides in L1 arrest and survival.

Supplementary Table 1. ^{1}H and ^{13}C NMR data derived from ^{1}H, dqf-COSY, HSQC, and HMBC spectra for nemamide A in dimethyl sulfoxide-d_6.

#	δ_H (J (Hz))	δ_C	HMBC
1		171.1	
2	4.51, m ($J_{2,3a}$ = 9.0; $J_{2,3b}$ = 6.9)	50.1	C_1
2-NH	7.46, brd ($J_{2,2\text{-NH}}$ = 8.1)		C_5
3a	2.45, overlap ($J_{3a,3b}$ = 15.9)	36.9	C_1, C_2
3b	2.61, overlap	36.9	C_1
4		171.3	
4-NH_2a	6.85, brs ($J_{4\text{-}NH_2a,4\text{-}NH_2b}$ = 4.8)		C_3
4-NH_2b	7.14, brs		C_4
5		170.7	
6	4.45, m ($J_{6,7a}$ = 4.9; $J_{6,7b}$ = 6.6)	49.3	
6-NH	8.42, brs ($J_{6,6\text{-NH}}$ = 8.2)		
7a	2.56, overlap ($J_{7a,7b}$ = 16.6)	35.8	C_5, C_8
7b	2.95, dd	35.8	C_6, C_8
8		173.3	
8-NH_2a	7.18, brs ($J_{8\text{-}NH_2a,8\text{-}NH_2b}$ = 4.9)		C_7
8-NH_2b	7.86, brs		
9		170.9	
10	4.22, m ($J_{10,11a}$ = 6.7; $J_{10,11b}$ = 9.6)	52.5	
10-NH	8.86, brs ($J_{10,10\text{-NH}}$ = 3.4)		
11a	2.44, overlap ($J_{11a,11b}$ = 17.8)	35.9	C_9, C_{12}
11b	2.53, overlap	35.9	C_9, C_{10}
12		173.1	
12-NH_2a	6.95, brs ($J_{12\text{-}NH_2a,12\text{-}NH_2b}$ = 4.8)		C_{11}
12-NH_2b	7.58, brs		
13		173.4	
14a	2.41, overlap ($J_{14a,15a}$ = 8.9)	33.3	C_{13}
14b	2.57, overlap ($J_{14a,14b}$ = 18.5)	33.3	C_{13}
15a	3.15, overlap ($J_{15a,15b}$ = 15.9)	34.8	
15b	3.42, overlap ($J_{14b,15b}$ = 9.6)	34.8	
15-NH	7.73, brs		
16		170.3	
17a	2.18, brd ($J_{17a,17b}$ = 14.5)	40.6	C_{16}
17b	2.47, overlap ($J_{17b,18}$ = 9.8)	40.6	C_{16}
18	4.08, m ($J_{18,19}$ =6.7)	44.9	
18-NH	7.05, brs ($J_{18,18\text{-NH}}$ = 8.2)		C_1
19	1.32, m ($J_{19,20}$ = 6.7)	43.7	C_{17}, C_{18}, C_{20}, C_{21}
20	3.51, m ($J_{20,21a}$ = 8.2)	63.3	
20-OH	4.55, brs		
21a	1.30, m ($J_{21a,21b}$ =14.5)	43.5	
21b	1.48, m ($J_{21b,22}$ = 9.8)	43.5	C_{22}
22	3.76, m ($J_{22,24}$ = 7.5)	77.6	C_{23}, C_{25}
23	3.13, s	55.5	C_{22}
24	5.51, dd ($J_{24,25}$ = 15.4)	133.7	C_{22}, C_{26}
25	6.19, dd ($J_{25,26}$ = 11.2)	131.3	C_{22}, C_{24}
26	6.14, dd ($J_{26,27}$ = 14.5)	129.7	C_{24}, C_{28}
27	6.23, dd ($J_{27,28}$ = 10.7)	132.9	C_{25}, C_{26}, C_{29}
28	6.07, dd ($J_{28,29}$ = 15.1)	130.1	C_{26}, C_{30}
29	5.72, dt ($J_{29,30}$ = 7.0)	135.2	C_{27}, C_{30}, C_{31}
30	2.06, m	32.0	C_{28}, C_{29}, C_{31}, C_{32}
31	1.35, overlap	28.2	C_{29}, C_{30}, C_{32}, C_{33}
32	1.24, overlap	30.8	C_{30}, C_{31}, C_{33}, C_{34}
33	1.26, overlap ($J_{33,34}$ = 7.1)	21.8	C_{31}, C_{32}, C_{34}
34	0.86, t	13.8	C_{32}, C_{33}

Supplementary Table 2. ^{1}H and ^{13}C NMR chemical shifts derived from ^{1}H, TOCSY, HSQC, and HMBC spectra for the three cyclic peptides in dimethyl sulfoxide-d_6.

#	Cyclic Peptide **3** (2*S*,6*R*,10*R*,18*R*)		Cyclic Peptide **4** (2*R*,6*S*,10*R*,18*S*)		Cyclic Peptide **5** (2*R*,6*R*,10*S*,18*S*)	
	δ_H (*J* (Hz))	δ_C	δ_H (*J* (Hz))	δ_C	δ_H (*J* (Hz))	δ_C
1		169.7		169.6		170.1
2	4.48, m	49.9	4.49, m	49.7	4.40, m	50.9
2-NH	7.49, brd, ($J_{2,2\text{-NH}}$ = 8.1)		7.85, brd, ($J_{2,2\text{-NH}}$ = 8.8)		7.49, brd, ($J_{2,2\text{-NH}}$ = 7.9)	
3a	2.43, dd, ($J_{3a,3b}$ = 19.4; $J_{2,3a}$ =12.7)	36.8	2.43, dd, ($J_{3a,3b}$ = 15.8; $J_{2,3a}$ =6.9)	35.1	2.56, overlap	36.5
3b	2.62, dd, ($J_{3a,3b}$ = 19.3; $J_{2,3b}$ =6.5)	36.8	2.69, ($J_{3a,3b}$ = 15.8; $J_{2,3b}$ =5.6)	35.1	2.56, overlap	36.5
4		171.2		171.8		171.2
4-NH_2a	6.82, brs		6.85, brs		6.88, brs	
4-NH_2b	7.11, brs		7.38, brs		7.27, brs	
5		170.5		170.3		170.7
6	4.41, m	49.2	4.40, m	48.7	4.33, m	50.9
6-NH	8.20, brd, ($J_{6,6\text{-NH}}$ = 8.8)		7.81, brd, ($J_{6,6\text{-NH}}$ = 8.8)		8.89, brd, ($J_{6,6\text{-NH}}$ = 5.2)	
7a	2.58, brd, ($J_{7a,7b}$ = 17.2)	35.4	2.54, overlap	35.3	2.48, overlap	35.4
7b	2.98, dd, ($J_{7a,7b}$ = 16.4; $J_{6,7b}$ =4.7)	35.4	3.05, dd, ($J_{7a,7b}$ = 17.2; $J_{6,7b}$ =3.8)	35.3	2.60, overlap	35.4
8		173.6		173.8		170.9
8-NH_2a	7.32, brs		7.47, brs		6.89, brs	
8-NH_2b	7.80, brs		7.92, brs		7.33, brs	
9		171.1		170.2		173.9
10	4.25, m	52.1	4.46, m	49.3	4.40, m	50.9
10-NH	8.63, brs		8.39, brd, ($J_{10,10\text{-NH}}$ = 7.4)		8.48, brs	
11a	2.51, overlap	35.6	2.48, overlap	35.4	2.31, brd, ($J_{11a,11b}$ = 16.1)	35.6
11b	2.51, overlap	35.6	2.65 , ($J_{11a,11b}$ = 15.7; $J_{10,11b}$ =6.8)	35.4	2.49, overlap	35.6
12		173.6		172.3		170.3
12-NH_2a	6.96, brs		6.95, brs		6.98, brs	
12-NH_2b	7.43, brs		7.33, brs		7.40, brs	
13		173.3		172.6		172.3
14a	2.42, overlap	33.5	2.36, m	34.7	2.23, m	34.0
14b	2.57, overlap	33.5	2.48, overlap	34.7	2.56, overlap	34.0
15a	3.18, m	34.8	3.14, overlap	34.3	3.33, overlap	35.4
15b	3.42, m	34.8	3.55, overlap	34.3	3.33, overlap	35.4
15-NH	7.36, brs		7.25, brs		7.00, brs	
16		170.7		170.2		170.0
17a	2.15, brd, ($J_{17a,17b}$ = 12.0)	41.4	2.11, brd, ($J_{17a,17b}$ = 11.3)	41.5	2.06, dd, ($J_{17a,17b}$ = 13.0, $J_{17a,18}$ = 9.4)	41.7
17b	2.46, overlap	41.4	2.51, oveerlap	41.5	2.36, brd, ($J_{17a,17b}$ = 13.1)	41.7
18	3.96, m	43.0	3.97, m	43.1	3.97, m	42.6
18-NH	6.95, brd, ($J_{18,18\text{-NH}}$ = 7.9)		7.08, overlap		6.66, brd, ($J_{18,18\text{-NH}}$ = 7.7)	
19	0.98, d, ($J_{18,19}$ = 5.9)	20.7	0.97, d, ($J_{18,19}$ = 5.9)	20.9	1.04, d, ($J_{18,19}$ = 6.5)	20.1

Supplementary Table 3. Differences between the cyclic peptides and nemamide A in terms of ^{1}H and ^{13}C NMR chemical shifts.*

#	$\delta_{H(peptide)}$- $\delta_{H(nemamideA)}$			$\delta_{C(peptide)}$- $\delta_{C(nemamideA)}$		
	Cyclic Peptide **3** (2*S*,6*R*, 10*R*,18*R*)	Cyclic Peptide **4** (2*R*,6*S*, 10*R*,18*S*)	Cyclic Peptide **5** (2*R*,6*R*, 10*S*,18*S*)	Cyclic Peptide **3** (2*S*,6*R*, 10*R*,18*R*)	Cyclic Peptide **4** (2*R*,6*S*, 10*R*,18*S*)	Cyclic Peptide **5** (2*R*,6*R*, 10*S*,18*S*)
1				-1.4	-1.5	-1
2	-0.03	-0.02	-0.11	-0.2	-0.4	0.8
2-NH	0.03	0.39	0.03			
3a	-0.02	-0.02	0.11	-0.1	-1.8	-0.4
3b	0.01	0.08	-0.05	-0.1	-1.8	-0.4
4				-0.1	0.5	-0.1
4-NH_2a	-0.03	0	0.03			
4-NH_2b	-0.03	0.24	0.13			
5				-0.2	-0.4	0
6	-0.04	-0.05	-0.12	-0.1	-0.6	1.6
6-NH	-0.22	-0.61	0.47			
7a	0.02	-0.02	-0.08	-0.4	-0.5	-0.4
7b	0.03	0.1	-0.35	-0.4	-0.5	-0.4
8				0.3	0.5	-2.4
8-NH_2a	0.14	0.29	-0.29			
8-NH_2b	-0.06	0.06	-0.53			
9				0.2	-0.7	3.0
10	0.03	0.24	0.18	-0.4	-3.2	-1.6
10-NH	-0.23	-0.47	-0.38			
11a	0.07	0.04	-0.13	-0.3	-0.5	-0.3
11b	-0.02	0.12	-0.04	-0.3	-0.5	-0.3
12				0.5	-0.8	-2.8
12-NH_2a	0.01	0	0.03			
12-NH_2b	-0.15	-0.25	-0.18			
13				-0.1	-0.8	-1.1
14a	0.01	-0.05	-0.18	0.2	1.4	0.7
14b	0	-0.09	-0.01	0.2	1.4	0.7
15a	0.03	-0.01	0.18	0	-0.5	0.6
15b	0	0.13	-0.09	0	-0.5	0.6
15-NH	-0.37	-0.48	-0.73			
16				0.4	-0.1	-0.3
17a	-0.03	-0.07	-0.12	0.8	0.9	1.1
17b	-0.01	0.04	-0.11	0.8	0.9	1.1
18	-0.12	-0.11	-0.11	-1.9	-1.8	-2.3
18-NH	-0.1	0.03	-0.39			
19	-0.34	-0.35	-0.28	-23	-22.8	-23.6

* ^{1}H and ^{13}C NMR chemical shifts of nemamide A (listed in Supplementary Table 1) were subtracted from the corresponding chemical shifts of the three cyclic peptides (listed in Supplementary Table 2). If $\delta_{H(cyclic\ peptide)}$- $\delta_{H(nemamideA)} > 0.1$, the value is highlighted in red. If $\delta_{C(cyclic\ peptide)}$- $\delta_{C(nemamideA)} > 1$, the value is highlighted in red. Exchangeable protons are shaded light gray as their chemical shifts vary depending on sample concentration ([cyclic peptide] >> [nemamide A]) and other factors. C-1, C-18, and C-19 rows are shaded dark gray as these values should be quite different between nemamide A and the three cyclic peptides, as the cyclic peptides were all truncated versions of nemamide A.

Supplementary Table 4. Comparison of the A domain selectivity codes. Selectivity codes for β-Ala and L-Asn in bacterial A domains are listed (in red). The corresponding amino acids in the PKS-1 A_1, NRPS-1 A_2, and NRPS-1 A_3 domains are listed for comparison.

Sequence position:	235	236	239	278	299	301	322	330	331	517
β-Ala recognition	V	D	X	V	I	S	X	G	D	K
L-Asn recognition	D	L	T	K	L	G	E	V	G	K
PKS-1 A_1	D	V	S	F	T	G	I	I	W	K
NRPS-1 A_2	D	I	A	Y	Q	G	E	V	Y	K
NRPS-1 A_3	D	N	L	L	I	G	N	A	F	K

Supplementary Table 5. Primers used for plasmid construction or genotyping.

Primer	Purpose	Sequence (5'-3')*
nrps-1p-AscI-F	GFP reporter	gcatGGCGCGCCTGCATCAGCACATACTCAATGGTC
nrps-1p-NotI-R	GFP reporter	catgGCGGCCGCTGTGCAGAGTGCTCCGCGTAG
pks-1p-SalI-F	GFP reporter	gcgcGTCGACTGTGCATACATGAGTTGTTGCT
pks-1p-NotI-R	GFP reporter	catgGCGGCCGCTTTCTCCAAATCTTAATACAAATTATAT
nrps-1-F	Mos1 detection	GGAGAAGTCATCTGTTTCCA
nrps-1-R	Mos1 detection	TTGGCGATCACTTCAAATGG
pks-1-F	Mos1 detection	GAGGGAATATTGTATCCCACC
pks-1-R	Mos1 detection	GAAAACCGTGTTTGGTCTCG
oJL115[19]	Mos1 detection	GCTCAATTCGCGCCAAACTATG
daf-16-F[20]	deletion detection	GTAGACGGTGACCATCTAGAG
daf-16-internal[20]	deletion detection	CGGGAATTTCAGCCAAAGAC
daf-16-R[20]	deletion detection	GACGATCCAGGAATCGAGAG
unc-31-F	deletion detection	TAAGACCGCCCATGTTGCAC
unc-31-internal	deletion detection	AGTTGTGGCCTCTCCAATTC
unc-31-R	deletion detection	ATTCTGAGGGCACGACTCTG
ins-11-F	qRT-PCR	TCTTCGTCAATGAGGGTCAAG
ins-11-R	qRT-PCR	CAGTCGGATGCTGTTCTCC

*Underlined bases indicate restriction sites.

References

1 Weber, T. *et al.* antiSMASH 3.0-a comprehensive resource for the genome mining of biosynthetic gene clusters. *Nucleic Acids Res* (2015).

2 Gowda, H. *et al.* Interactive XCMS Online: simplifying advanced metabolomic data processing and subsequent statistical analyses. *Anal Chem* **86**, 6931-6939 (2014).

3 Nugroho, A. E. & Morita, H. Circular dichroism calculation for natural products. *J Nat Med* **68**, 1-10 (2014).

4 Lu, Z. *et al.* Cytotoxic polyphenols from the marine-derived fungus *Penicillium expansum*. *J Nat Prod* **73**, 911-914 (2010).

5 Wu, Q. X. *et al.* Azonazine, a novel dipeptide from a Hawaiian marine sediment-derived fungus, *Aspergillus insulicola*. *Org Lett* **12**, 4458-4461 (2010).

6 Liu, X. F. *et al.* Simplextones A and B, unusual polyketides from the marine sponge *Plakortis simplex*. *Org Lett* **13**, 3154-3157 (2011).

7 Kwan, D. H. & Schulz, F. The stereochemistry of complex polyketide biosynthesis by modular polyketide synthases. *Molecules* **16**, 6092-6115 (2011).

8 Reid, R. *et al.* A model of structure and catalysis for ketoreductase domains in modular polyketide synthases. *Biochemistry* **42**, 72-79 (2003).

9 Sievers, F. *et al.* Fast, scalable generation of high-quality protein multiple sequence alignments using Clustal Omega. *Mol Syst Biol* **7**, 539 (2011).

10 Kotowska, M. & Pawlik, K. Roles of type II thioesterases and their application for secondary metabolite yield improvement. *Appl Microbiol Biotechnol* **98**, 7735-7746 (2014).

11 Tamura, K., Stecher, G., Peterson, D., Filipski, A. & Kumar, S. MEGA6: Molecular Evolutionary Genetics Analysis version 6.0. *Mol Biol Evol* **30**, 2725-2729 (2013).

12 Baugh, L. R. & Sternberg, P. W. DAF-16/FOXO regulates transcription of *cki-1*/Cip/Kip and repression of *lin-4* during *C. elegans* L1 arrest. *Curr Biol* **16**, 780-785 (2006).

13 Fukuyama, M., Kontani, K., Katada, T. & Rougvie, A. E. The *C. elegans* Hypodermis Couples Progenitor Cell Quiescence to the Dietary State. *Curr Biol* **25**, 1241-1248 (2015).

14 Fukuyama, M., Rougvie, A. E. & Rothman, J. H. *C. elegans* DAF-18/PTEN mediates nutrient-dependent arrest of cell cycle and growth in the germline. *Curr Biol* **16**, 773-779 (2006).

15 Fukuyama, M. *et al. C. elegans* AMPKs promote survival and arrest germline development during nutrient stress. *Biol Open* **1**, 929-936 (2012).

16 Chen, Y. & Baugh, L. R. *Ins-4* and *daf-28* function redundantly to regulate *C. elegans* L1 arrest. *Dev Biol* **394**, 314-326 (2014).

17 Baugh, L. R. To grow or not to grow: nutritional control of development during *Caenorhabditis elegans* L1 arrest. *Genetics* **194**, 539-555 (2013).

18 Lee, B. H. & Ashrafi, K. A TRPV channel modulates *C. elegans* neurosecretion, larval starvation survival, and adult lifespan. *PLoS Genet* **4**, e1000213 (2008).

19 Boulin, T. & Bessereau, J. L. Mos1-mediated insertional mutagenesis in *Caenorhabditis elegans*. *Nat Protoc* **2**, 1276-1287 (2007).

20 Jeong, M. H., Kawasaki, I. & Shim, Y. H. A circulatory transcriptional regulation among *daf-9*, *daf-12*, and *daf-16* mediates larval development upon cholesterol starvation in *Caenorhabditis elegans*. *Dev Dyn* **239**, 1931-1940 (2010).